© 2022. Published by The Company of Biologists Ltd | Journal of Cell Science (2022) 135, jcs260511. doi:10.1242/jcs.260511

RESEARCH ARTICLE

Release of HIV-1 particles from macrophages is promoted by an anchored cytoskeleton and driven by mechanical constraints

Vasco Rodrigues[1,*], Sarah Taheraly[1], Mathieu Maurin[1], Mabel San-Roman[2], Emma Granier[1], Anaël Hanouna[1] and Philippe Benaroch[1,*]

ABSTRACT

A feature of HIV-1 replication in macrophages is that viral assembly occurs at the limiting membrane of a compartment often named the virus-containing compartment (VCC). Assembled virions accumulate in the lumen of the VCC, from where they can be released into the extracellular medium via mechanisms that remain poorly described. Here, we show that the actin cytoskeleton contributes to this process by performing experiments combining pharmacological and mechanical perturbations with imaging and biochemical analysis. We found that jasplakinolide inhibited HIV-1 release from macrophages and led to scattering of the compartment. Concomitantly, both the integrin CD18 (β2-integrin) and the phosphorylated form of PYK2 (also known as PTK2B) were displaced away from the VCC. Inhibition of PYK2 activity promoted retention of viral particles in VCCs that lost their connections to the surface. Finally, in infected macrophages undergoing frustrated phagocytosis, VCCs rapidly trafficked to the basal membrane and released their viral content, in a manner dependent on their association with the actin cytoskeleton. These results highlight that the trafficking of VCCs and virus release are intimately linked to a reorganization of the macrophage actin cytoskeleton that can be modulated by external physical cues.

KEY WORDS: HIV, Actin, Macrophage, Viral release, Viral-containing compartment

INTRODUCTION

Macrophages are embedded in many tissues where they ensure specific functions. Early studies established that HIV-1-infected patients possess infected macrophages in many of their tissues (Orenstein et al., 1988). Usage of monocyte-derived macrophages (MDMs) exposed to HIV-1 *in vitro* allowed the study of the viral replication cycle and revealed some of its specific features as compared to how it replicated in T lymphocytes (Rodrigues et al., 2017; Sattentau and Stevenson, 2016). Viral assembly takes place in macrophages at the limiting membrane of a compartment that appears intracellular. The newly formed virions, pinch off from this membrane in the lumen of the compartment, which is hence called a virus-containing compartment (VCC), where they accumulate. Interestingly, compartments with very similar characteristics are also present in uninfected macrophages, as they similarly express tetraspanins (CD9, CD81 and CD53) (Deneka et al., 2007), and the scavenger receptor CD36 (Berre et al., 2013), and are often designated intracellular plasma membrane-connected compartments (IPMCs). Upon HIV-1 infection, newly synthesized Gag is recruited to these pre-existing compartments, which then become *de facto* VCCs (Berre et al., 2013).

The VCC and IPMC possess a very intricate architecture and are often connected to the extracellular medium by channels or conduits that are too narrow to allow the virions to exit but that permit fluid exchanges (Gaudin et al., 2013; Welsch et al., 2007). They remain mostly inaccessible to macromolecules delivered from the extracellular medium, such as antibodies (Chu et al., 2012). The precise nature of the VCC has been debated but the current view holds that it originates from tetraspanin-rich zones of the plasma membrane that have been internally sequestered. Although VCCs are generally considered as continuous with the plasma membrane, recent work also suggests that they can be completely enclosed compartments that could fuse with plasma membrane-connected compartments (Ladinsky et al., 2019). These studies highlight a rather complex and dynamic structure that results in a more complex release of viral particles as compared with other cell types.

How the virions stocked in the VCC lumen are released in the extracellular medium remains an open question. Exposure of an infected MDM to extracellular ATP (eATP) prompts a rapid discharge of the viral particles stored in the VCC, via stimulation of the P2X7 purinergic receptor (Graziano et al., 2015). The rapid and drastic remodelling of the cell shape and actin cytoskeleton that eATP induces in HIV-infected MDMs might underlie its impact on viral release. This interpretation raises the question of how the structure of VCCs, their trafficking, and consequently viral particle release are impacted by or depend on the actin cytoskeleton.

The VCC is surrounded by a meshwork of filamentous actin tightly associated with its external membrane (Mlcochova et al., 2013; Pelchen-Matthews et al., 2012), which is often decorated by an electron dense molecular coat that appears to anchor the actin cytoskeleton to the compartment (Pelchen-Matthews et al., 2012). These coats have striking resemblances with focal adhesions, as they contain the β2-integrin CD18 and its associated CD11b (integrin αM) and CD11c (integrin αX) α-integrins. Focal adhesion linker proteins, such as talins, vinculin and paxillin are also found at these molecular coats (Pelchen-Matthews et al., 2012). Silencing CD18 in HIV-1 infected macrophages did not alter viral release over a 24-h window (Pelchen-Matthews et al., 2012). Whether a longer period of analysis impacts viral release was not assessed; nevertheless, CD18 silencing led to scattering of the VCC across the cell (Pelchen-Matthews et al., 2012), suggesting that these coats are an integral part of the compartment. Also, during direct transmission of HIV-1 from infected macrophages to CD4T cells, the VCCs become polarized toward the cell–cell interface, or viral synapse, in an actin cytoskeleton-dependent manner (Duncan et al., 2014).

[1]Institut Curie, PSL Research University, INSERM U932, Immunity and Cancer, 75005 Paris, France. [2]Institut Curie, UMR3215, 75005 Paris, France.

*Authors for correspondence (vteixeir@curie.fr; Philippe.Benaroch@curie.fr)

V.R., 0000-0002-6014-321X; A.H., 0000-0001-9271-5094

Handling Editor: Michael Way
Received 11 August 2022; Accepted 12 August 2022

Journal of Cell Science (2022) 135, jcs260511. doi:10.1242/jcs.260511

In macrophages, many focal adhesion-mediated processes, such as cell migration, are regulated by focal adhesion kinase (FAK; also known as PTK2)-related proline-rich tyrosine kinase 2 (PYK2; also known as PTK2B) (Okigaki et al., 2003). PYK2 promotes the assembly of focal adhesions at the leading edge, and their disassembly at the trailing edge to ensure net forward movement (Zhu et al., 2018). The full breadth of PYK2 activators and substrates remain incompletely understood, but it is generally considered to act at the crossroads between integrin and small GTPases, such as those of Rho family (Schaller, 2010).

It remains unclear how the VCC structure and HIV particle release are impacted by these focal adhesion-like coats and PYK2 signalling and, in general, our understanding on how the actin cytoskeleton impacts HIV release from macrophages remains rudimentary. We report here that pharmacological stabilization of actin fibres led to scattering of the VCC and reduced viral particle release from infected MDMs. This was paralleled by decreased association of the integrin CD18 and of the phosphorylated form of the kinase PYK2 with the compartment. Specific inhibition of PYK2 led to accumulation of viral particles in VCCs that lost their connection to the plasma membrane. Finally, subjecting infected MDMs to frustrated phagocytosis on glass coverslip induced rapid trafficking of VCCs to the surface and viral release. Such trafficking required the compartment to be associated with CD18 and the actin cytoskeleton. We propose that focal adhesion-like coats are regulated by PYK2 and anchor the actin cytoskeleton to the VCC to promote HIV release from macrophages.

RESULTS

Actin dynamics modulate viral particle release from HIV-1-infected macrophages

In MDMs infected with HIV-1-GAG-iGFP-ΔENV-VSVG for 4 days, phalloidin staining can be readily observed around the VCC, confirming previous observations (Mlcochova et al., 2013) (Fig. 1A,B). F-actin appears to be docked at or surrounding the compartment (see 3D panel in Fig. 1B). Ultrastructural analysis by electron microscopy (EM) revealed the presence of actin filaments anchored at and radiating from the VCC (Fig. S1A–C). Live imaging of MDMs transduced with Lifeact–mCherry and infected with HIV-1-GAG-iGFP-ΔENV-VSVG confirmed that the VCC and the actin cytoskeleton are in proximity to each other and exhibit synchronized movements (Fig. 1C; Movie 1).

We next turned to pharmacological manipulation of the actin cytoskeleton of infected macrophages to ascertain how it impacts VCC size and structure as well as viral release.

We infected MDMs with HIV-1-ΔENV-VSVG for 4 days to allow formation of VCCs and treated them with a panel of pharmacological modulators of the actin cytoskeleton. After 24 h, we observed that the F-actin stabilizing drug, jasplakinolide, reduced the release of viral particles (Fig. 1D), as measured by our in-house cytometric bead array (CBA) assay, which specifically detects the HIV-1 p24 capsid protein (Fig. S1D–F). None of the other cytoskeleton-modifying drugs had significant effects on viral release over the 24-h period (Fig. 1D). Jasplakinolide was also the sole drug to induce retention of p24 inside the macrophage during the 24-h treatment period, suggesting that the viral particles are retained inside the cell, hence their decreased concentration in the supernatant (Fig. 1E–G). Interestingly, treatment of HIV-1-infected HeLa cells with the same cytoskeleton modulators failed to induce any significant changes in p24 release over vehicle-treated cells (Fig. S1G), suggesting that the effect of jasplakinolide treatment on viral release specifically impacts macrophages.

Stabilization of actin fibres impacts the VCC structure and architecture

We next asked how jasplakinolide treatment results in retention of p24 in the macrophage, by examining its impact on the VCC by confocal microscopy. MDMs were infected with HIV-1-GAG-iGFP-ΔENV-VSVG for 4 days, treated or not with a non-toxic dose of jasplakinolide for 24 h and analysed by confocal microscopy. As expected, the drug had a strong impact on the general macrophage morphology, as cells rounded up and lost their typical spreading over the substrate (Fig. 2A). Although this led to a significant decrease in cell spreading (Fig. 2B), treatment with jasplakinolide increased the total volume of the VCC by more than 2-fold (Fig. 2C). The average intensity of the Gag-iGFP signal was similar between treated and not treated cells (Fig. 2D), although the compartment spread more evenly throughout the cell (Fig. 2E). These observations were confirmed by EM, as the typical VCC in vehicle-treated cells appear to fragment into smaller, but more numerous, compartments after treatment with jasplakinolide (Fig. 2F). Jasplakinolide-treated MDMs also exhibited massive accumulations of F-actin that occupied large sections of the cytoplasm (Fig. 2F, bottom left panel). Their appearance is concomitant with loss of the actin filaments that typically radiate from the VCC in control macrophages.

Shorter exposure of infected MDMs to jasplakinolide (2 h or 8 h) similarly resulted in cells rounding up (Fig. S2A,B) and a tendency for increased volume and dispersion of the VCC, although without statistical significance (Fig. S2C–E), likely due to the strong heterogeneity of the compartment. Live-cell imaging confirmed the strong impact that jasplakinolide has on both MDM morphology and VCC properties, and that such effects can occur rapidly (Fig. S2F; Movie 2). However, individual cells likely do not respond synchronously to the drug which led us to choose a 24-h incubation to further analyse the impact of manipulating the actin cytoskeleton on the VCC, as at this timepoint most or all cells have responded to the drug.

In an additional set of experiments (Fig. S3A), we observed that an infectious strain of HIV-1 (NL-AD8) similarly induces viral compartments in macrophages that associate with F-actin (Fig. S3B) and become dispersed when exposed to jasplakinolide (Fig. S3C), indicating that this phenotype is preserved in fully infectious enveloped virus.

We also observed that the other actin modulators that failed to alter viral release (mycalolide B, CK666 and blebbistatin; Fig. 1D) also did not significantly alter the VCC characteristics at the concentrations and time-of-exposure tested (Fig. S4A–D). Actin depolymerization with mycalolide B led to shrinkage and rounding up of the macrophage (Fig. S4A,B), although without significant effects on VCC volume (Fig. S4A,C,D).

Overall, these data suggest that drug-induced F-actin stabilization leads to loss of the organized actin filaments that are anchored at the VCC. Consequentially, compartments become dispersed throughout the cell and accumulate, resulting in impaired viral release.

Stabilization of actin fibres relocalizes the integrin CD18 away from the VCC-limiting membrane

Previous work has reported that the β2-integrin CD18 is present in focal adhesion-like electron-dense regions at the limiting membrane of the VCC and is critical for the integrity of the VCC (Pelchen-Matthews et al., 2012). We confirmed the presence of electron-dense regions that coat the VCC and that serve as anchoring sites for the actin cytoskeleton (Fig. 3A; Fig. S1A,B). These coats were

Journal of Cell Science (2022) 135, jcs260511. doi:10.1242/jcs.260511

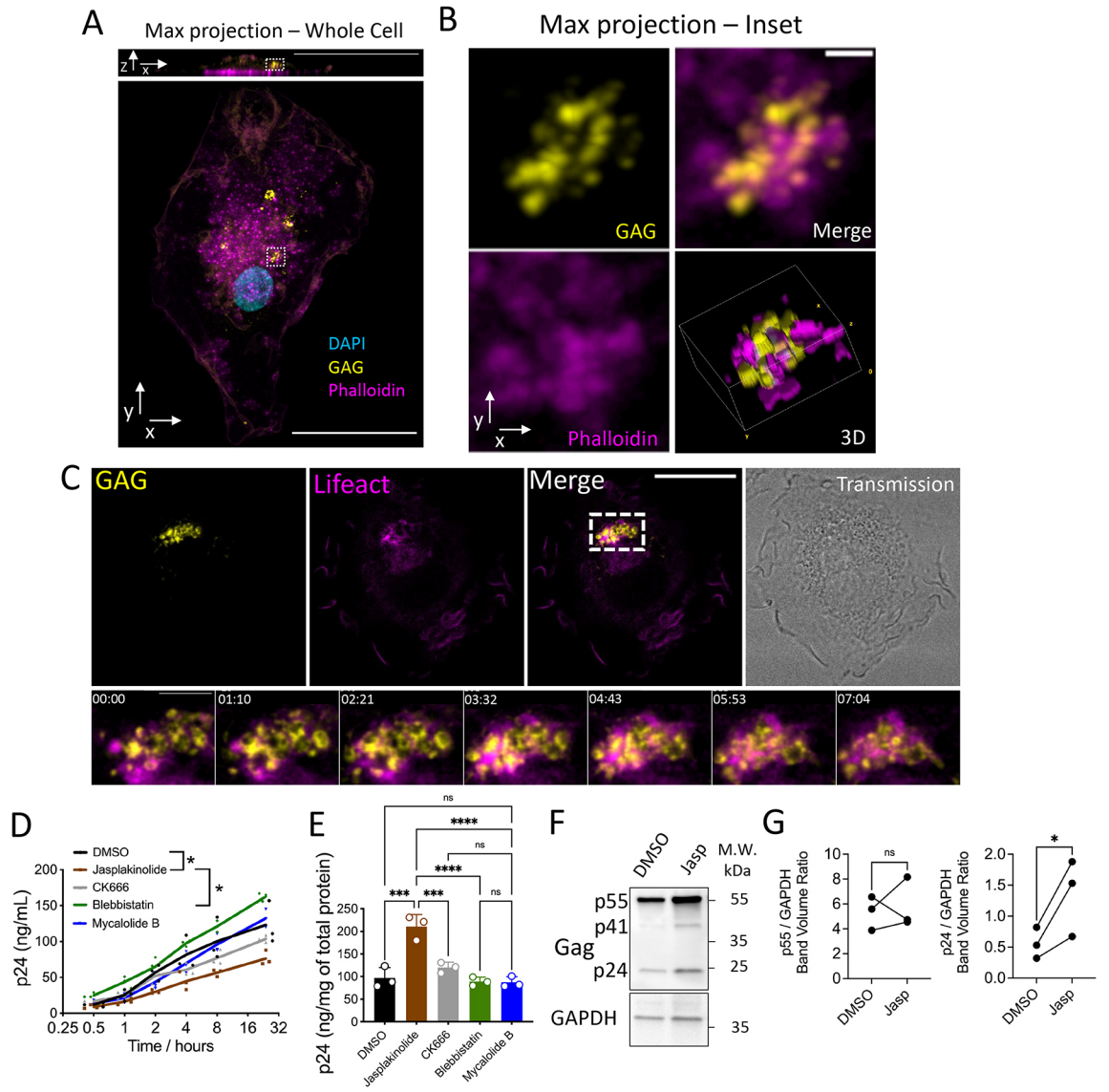

Fig. 1. Actin is involved in VCC dynamics and viral release from macrophages. (A) MDMs infected with HIV-1-GAG-iGFP-ΔENV-VSVG for 7 days, stained for phalloidin. The bottom panel shows a maximum intensity *z*-projection. The top panel shows a slice on the *xz* plane, highlighting the selected region for B. Neighbouring cells were manually removed from the original image for clarity. Scale bars: 30 µm. (B) Maximum intensity *z*-projection and 3D volume rendering of the region highlighted in 1A. Scale bar: 1 µm. (C) MDMs transduced with Lifeact–mCherry were infected with HIV-1-GAG-iGFP-dENV-VSVG (MOI=1.0). Time-lapse imaging was performed at day 6 after infection; times shown are in minutes and seconds. The bottom panels represent the region in the dashed box in the top panels. Scale bars: 20 µm (top panels) and 5 µm (bottom panels). Images shown in A–C are representative of three experiments. (D) MDMs were infected with HIV-1-ΔENV-VSVG at a MOI=1.0 for 4 days. Cells were subsequently treated with the indicated drugs for 24 h. Supernatant aliquots were recovered at the indicated time-points, and the released p24 was quantified by a custom-made CBA assay. Jasplakinolide was used at 50 nM; CK666 was used at 10 µM; blebbistatin was used at 5 µM; mycalolide-B was used at 100 nM. Data from three independent donors. **P*<0.05 (two-way ANOVA with Tukey's post test). (E) As in D, cells were lysed at the end of the experimental procedure in NP-40 lysis buffer and intracellular p24 was quantified by means of a CBA. Data from three independent donors and shown as mean±s.d. ****P*<0.001; *****P*<0.0001; ns, not significant (one-way ANOVA with Dunnett's multiple comparisons test). (F) As in D, cells were lysed in RIPA buffer at the end of the experimental procedure and analysed by western blot for the expression of GAG. One representative donor is shown. (G) Densitometry quantification of the western blot bands from F for three independent donors. **P*<0.05; ns, not significant (paired two-tailed *t*-test).

also present in VCCs at, or close to, the cell surface (Fig. 3B), implicating them in the trafficking of the compartment. Confocal immunofluorescence confirmed that CD18 surrounds the VCC (Fig. 3C,D). However, treatment with jasplakinolide led to a significant decrease in the enrichment of CD18 in the vicinity of the VCC (Fig. 3C,D). Analysis by EM confirmed that the electron-dense coats typical of control MDMs, were no longer observable in the smaller and more numerous VCCs of jasplakinolide-treated cells (Fig. 3E,F). Our data indicate that pharmacological stabilization of actin leads VCCs to lose their association with focal adhesion-like coats and the integrin CD18, which possibly underlies the accumulation of viral particles inside the cell.

The phosphorylated form of the focal adhesion kinase PYK2 localizes at the VCC

Because of the similarities between focal adhesions and the electron-dense coats around the VCC, we evaluated whether PYK2, a non-receptor tyrosine focal adhesion kinase (FAK) that

Journal of Cell Science (2022) 135, jcs260511. doi:10.1242/jcs.260511

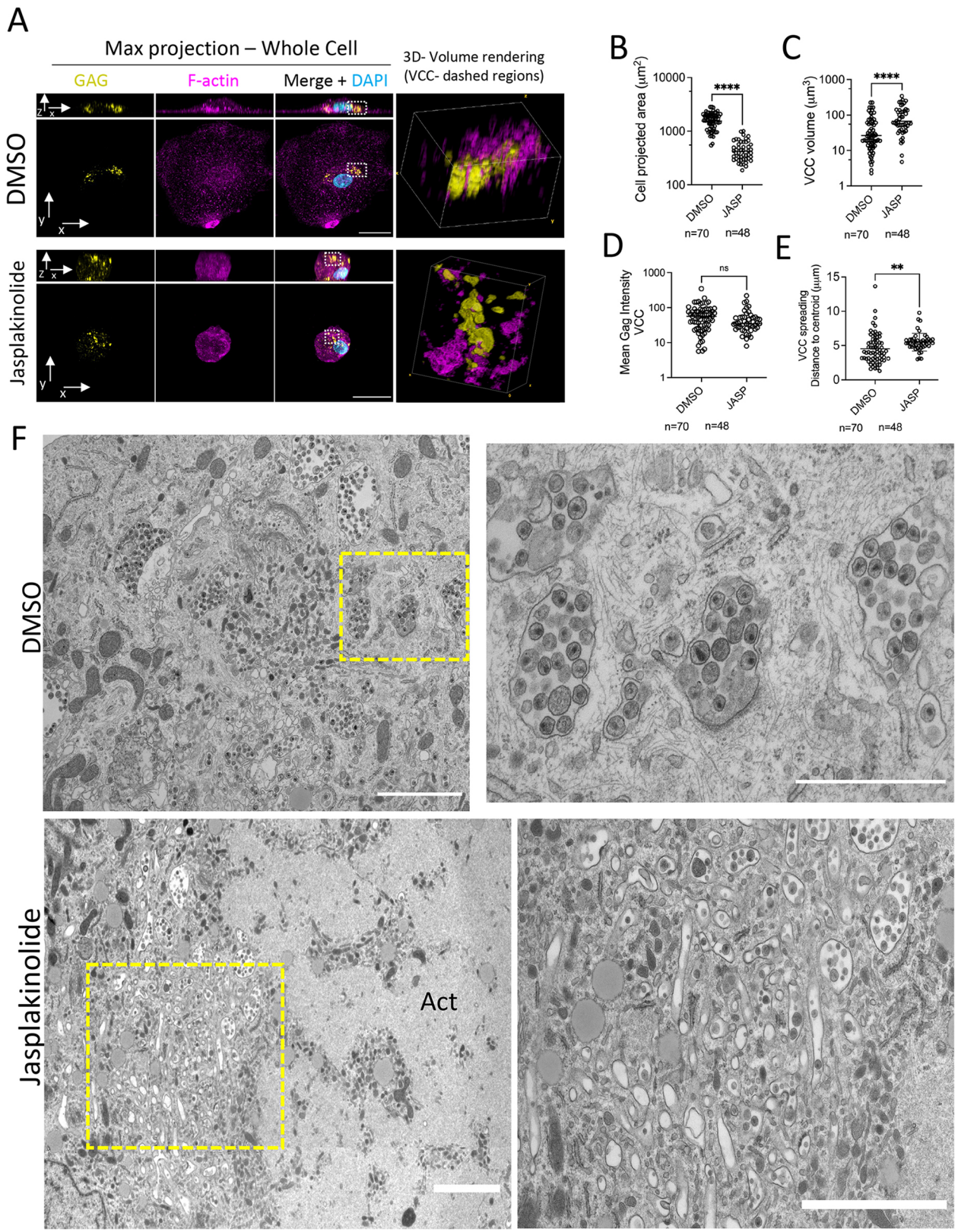

Fig. 2. Stabilization of actin fibres scatters the VCC and increases the total volume of the compartment. (A) MDMs were grown on coverslips, infected with HIV-1-ΔENV-GAG-iGFP-VSVG at a MOI=1.0 for 4 days and subsequently treated with DMSO or jasplakinolide (100 nM) for 24 h. Cells were fixed, stained for anti-F-actin and imaged by confocal microscopy. Neighbouring cells were manually removed from the original image for clarity. Scale bars: 20 µm. (B–E) Image analysis for cells processed as in A for the indicated parameters. See Materials and Methods for details on the quantification strategies employed. Each circle represents one cell, and the mean is indicated; the plots display cells from three independent donors. ***P*<0.01; *****P*<0.0001; ns, not significant (unpaired two-tailed *t*-test). (F) Cells were treated as in A and processed for electron microscopy. The right panels are enlargements of the areas enclosed in the dashed boxes on the left panels. Images shown in F are representative of three independent donors. Scale bars: 2 µm (left panels), 1 µm (right panel).

Journal of Cell Science (2022) 135, jcs260511. doi:10.1242/jcs.260511

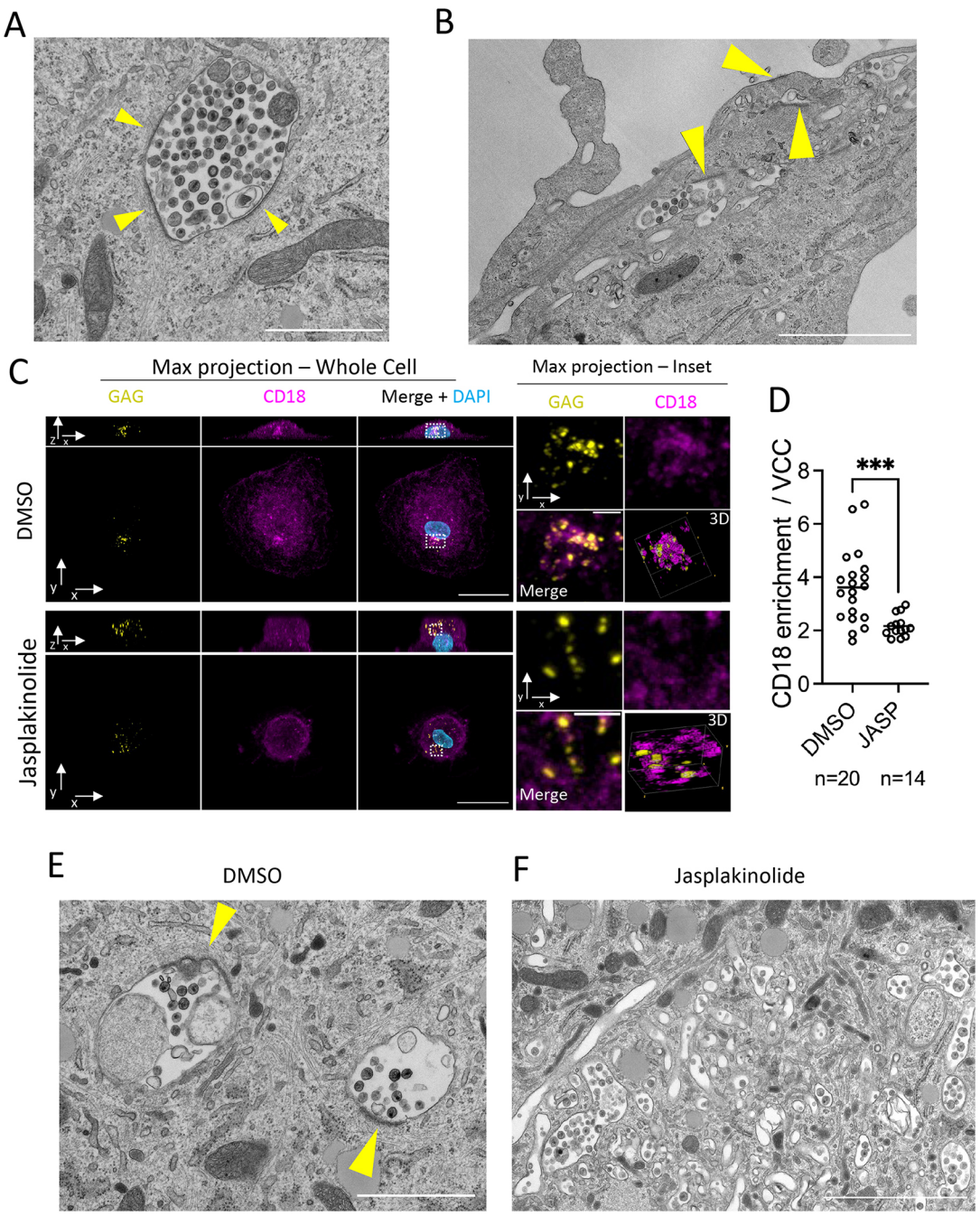

Fig. 3. Stabilization of actin fibres relocalizes the integrin CD18 away from the VCC limiting membrane in HIV-1-infected macrophages. (A,B) MDMs were infected HIV-1-ΔENV-VSVG (MOI=1.0) for 7 days. Cells were fixed and processed for electron microscopy. A depicts an example of an internal VCC with associated electron-dense coats. B highlights the presence of compartments with coats close to the cell surface. Arrowheads point to the electron-dense coats. Scale bars: 2 µm (C) Confocal microscopy of MDMs infected with HIV-1-Gag-iGFP-ΔENV-VSVG (MOI=1.0) for 4 days and treated with jasplakinolide or DMSO for 24 h. Whole-cell projections are shown on the right, along the *z*-axis (bottom) or the *y*-axis (top). The areas enclosed in the dashed boxes are enlarged and shown as *z*-projections on the right. Scale bars: 20 µm (left panels), 2 µm (right panels). (D) Quantification of CD18 enrichment at the VCC by image analysis. Each dot represents a single cell from three independent donors. See Materials and Methods for details on the analysis. ***P<0.001 (unpaired two-tailed *t*-test). (E,F) Electron microscopy of MDMs infected with HIV-1-ΔENV-VSVG (MOI=1.0) for 4 days and treated with jasplakinolide or DMSO for 24 h. Arrowheads point to electron-dense regions associated with the VCC in DMSO-treated cells (note their absence in cells treated with jasplakinolide). Scale bars: 2 µm. Images shown in A,B,E,F are representative of three independent donors.

governs the focal adhesion response to integrin-mediated signalling, plays a role in regulating the VCC structure and HIV-1 release from macrophages. Confocal microscopy revealed that the active, Tyr-402 phosphorylated, form of PYK2 [P-PYK2 (Y402)] localized mostly to the basal surface of the macrophage and was organized into large clusters that likely corresponded to podosomes (Fig. 4A,B, top panels). However, a pool of P-PYK2 colocalized with CD18 at the VCC in MDMs infected with HIV-1-Gag-iGFP-ΔEnv-VSVG (Fig. 4A,B, top panels). Jasplakinolide treatment for 24 h led to a dispersion of the P-PYK2 signal throughout the cell (Fig. 4B, bottom panels) and loss of the enrichment of P-PYK2 at the VCC observed in vehicle-treated cells (Fig. 4C).

Journal of Cell Science (2022) 135, jcs260511. doi:10.1242/jcs.260511

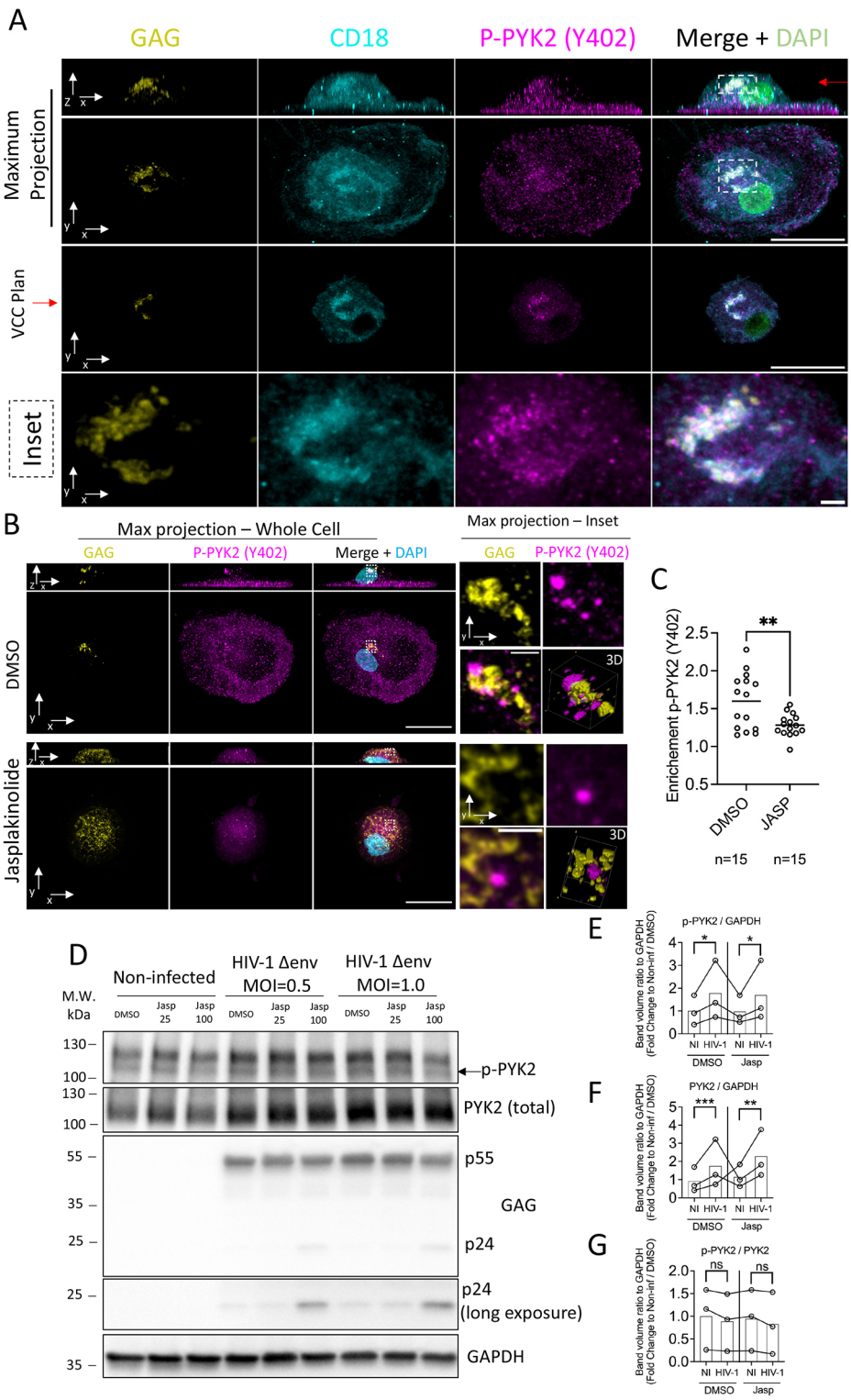

Fig. 4. The phosphorylated form of integrin-associated kinase PYK2 partially colocalizes with the VCC. (A) Confocal microscopy of MDMs infected with HIV-1-Gag-iGFP-ΔENV-VSVG (MOI=1.0) for 7 days and imaged for Gag–iGFP, CD18 and P-PYK2. The top panels show maximum projections across the *y*-axis. The second row shows maximum projections across the *z*-axis. The third row from the top shows a single *z*-slice at the level of the VCC (indicated by the red arrow in the top panel). The bottom row shows a magnification of the VCC region, as defined by the dashed regions in the top two panels. Scale bars: 20 µm (second and third rows from the top), 2 µm (bottom row). (B) Confocal microscopy of MDMs infected with HIV-1-Gag-iGFP-ΔENV-VSVG (MOI=1.0) for 4 days and treated with 50 nM jasplakinolide or DMSO for 24 h. Whole-cell projections are shown on the left, along the *z*-axis (bottom) or the *y*-axis (top). The areas enclosed in the dashed boxes are enlarged and shown as *z*-projections on the right. Scale bars: 20 µm (left panels), 2 µm (right panels). (C) Quantification of P-(Y402)-PYK2 enrichment at the VCC by image analysis. Each dot represents a single cell from two independent donors. See Materials and Methods for details on the analysis. $^{**}P<0.01$ (unpaired two-tailed *t*-test). (D) MDMs left uninfected (NI) or infected with HIV-1-Δ-ENV-VSVG (MOI=0.5 or 1.0) for 4 days were treated with jasplakinolide (25 or 100 nM) or vehicle (DMSO) for 24 h. Cells were lysed and analysed by western blot for the indicated proteins. (E–G) Quantification of western blot band density for three donors processed as in D. Each plot compares band density between non-infected and HIV-1-infected (MOI=1.0) MDMs from paired samples (same donor) for vehicle or jasplakinolide-treated samples. The average from the three donors for the control condition (non-infected/DSMO) was normalized to 1 and values are presented as fold change to this control condition. (E) P-PYK2 (Y402), (F) Total PYK2 and (G) P-PYK2/total PYK2. $^{*}P<0.05$; $^{**}P<0.01$; $^{***}P<0.001$; ns, not significant (paired two-tailed *t*-test).

Jasplakinolide treatment did not alter the levels of P-PYK2 and total PYK2 in both infected and non-infected MDMs (Fig. 4D). In contrast, both the total levels of PYK2 and P-PYK2 are significantly increased after HIV-1 infection of MDMs, although the ratio P-PYK2/total PYK2 remained stable (Fig. 4D–G). Collectively, our data indicates increased expression of PYK2 after macrophage infection with HIV-1 and that jasplakinolide treatment induces loss of association of the phosphorylated form of PYK2 from the VCC, accompanying the loss of CD18 and focal adhesion-like coats.

Active PYK2 participates in viral particle release from the VCC

Overall, our results hint at a possible role for PYK2 as a coordinator of the actin dynamics at the VCC, given that (1) its active phosphorylated form localizes to the compartment, (2) jasplakinolide treatment disrupts its localization at the VCC, concomitant with loss of the electron-dense regions and CD18 expression at the compartment, and (3) HIV-1 infection of MDMs induces an increase in the expression of both P-PYK2 and total

Journal of Cell Science (2022) 135, jcs260511. doi:10.1242/jcs.260511

PYK2. To directly test this hypothesis, we treated HIV-1-ΔENV-infected MDMs with PF431396 (PF396), a dual FAK and PYK2 inhibitor that has higher affinity for PYK2 over FAK (IC_{50} values of 2 and 11 nM, respectively; Han et al., 2009). Treatment of infected MDMs for 4 days with PF396 did not impede the upregulation of total PYK2 in infected MDMs (Fig. 5A,C), although it prevented the increase in P-PYK2 (Y402) observed after HIV-1 infection in vehicle-treated cells (Fig. 5A,B,D). Interestingly, PYK2 inhibition

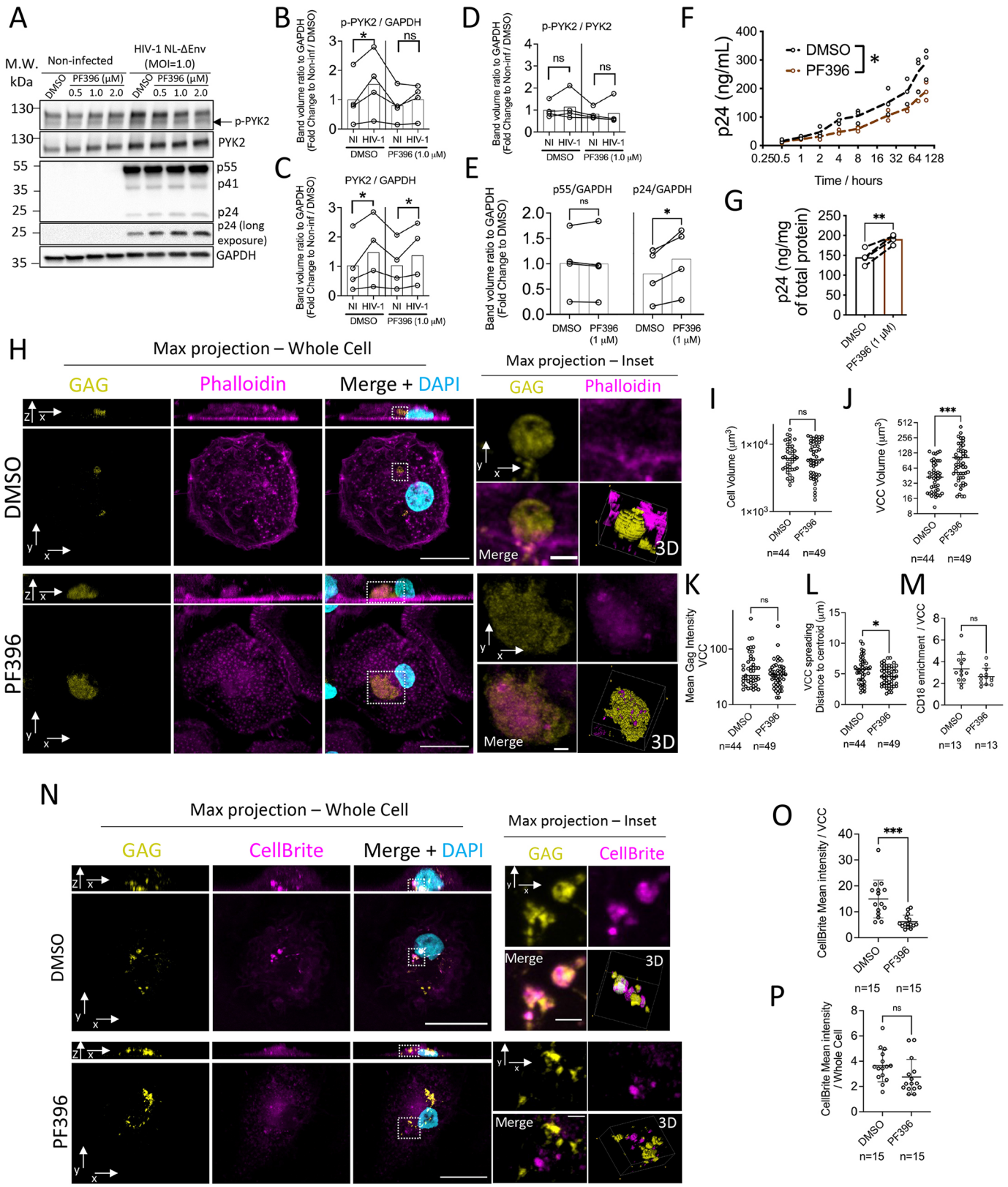

Fig. 5. See next page for legend.

Journal of Cell Science (2022) 135, jcs260511. doi:10.1242/jcs.260511

Fig. 5. A PYK2 inhibitor promotes HIV-1 retention in VCC. (A) MDMs left uninfected (NI) or infected with HIV-1-Δ-ENV-VSVG (MOI=1.0) for 4 days were treated with increasing doses of PF396 (0.5, 1.0 or 2.0 µM) or vehicle (DMSO) for additional 96 h. Cells were lysed and analysed by western blot with the indicated antibodies. (B–E) Quantification of western blot band density for four donors processed as in A. B–D compare band density for the proteins indicated in the plot title between non-infected and HIV-1-infected (MOI=1.0) MDMs from paired samples (same donor) for vehicle or PF396 (1 µM)-treated samples. In E, band intensity for p55 and p24 is compared between vehicle-treated and PF396-treated cells. The average from the four donors for the control condition (non-infected/DMSO for B,C; HIV-1/DMSO for E) was normalized to 1 and values are presented as fold change to the control condition. *P<0.05; ns, not significant (paired two-tailed t-test). (F) MDMs were infected with HIV-1-ΔENV-VSVG at a MOI=1.0 for 4 days. Cells were subsequently treated with PF396 (1 µM). At the indicated timepoints, supernatant aliquots were recovered, and the released p24 was quantified by CBA. Data from three independent donors. *P<0.05 (two-way ANOVA with Tukey's post test). (G) As in B, cells were lysed at the end of the experimental procedure in NP-40 lysis buffer and intracellular p24 was quantified by CBA. Data from three independent donors. **P<0.01 (paired two-tailed t-test). (H) Confocal microscopy of MDMs infected with HIV-1-Gag-iGFP-ΔENV-VSVG (MOI=1.0) for 4 days and treated with PF396 (1 µM) or vehicle (DMSO) for an additional 96 h. Whole-cell projections are shown on the left, along the z-axis (bottom) or the y-axis (top). The areas enclosed in the dashed boxes are magnified and shown as z-projections on the right. Scale bars: 20 µm (left panels), 2 µm (right panels). (I–L) Image analysis for cells processed as in D for the indicated parameters. See Materials and Methods for details on the quantification strategies employed. Each circle represents one cell, and the plots show cells from three independent donors. *P<0.05; ***P<0.001; ns, not significant (unpaired two-tailed t-test). (M) CD18 enrichment at the VCC for cells processed as in Fig. S4. See Materials and Methods for details on image analysis. Each circle represents one cell, and the plots display cells from two independent donors (mean±s.d.). ns, not significant (unpaired two-tailed t-test). (N) Confocal microscopy of MDMs infected with HIV-1-Gag-iGFP-ΔENV-VSVG (MOI=1.0) for 4 days and treated with PF396 (1 µM) or vehicle (DMSO) for additional 96 h. Cells were exposed to CellBrite before fixation. The left panels show whole-cell projections along the z-axis (bottom) or the y-axis (top). Magnifications of the areas enclosed in the dashed squares are shown as z-projections on the right. Scale bars: 20 µm (left panels), 2 µm (right panels). (O,P) Quantification (mean±s.d.) of CellBrite intensity in the VCC (O) or elsewhere in the cell (P) for cells processed as in K. See Materials and Methods for details. Each circle represents one cell, and the plots show cells from two independent donors. ***P<0.001; ns, not significant (unpaired two-tailed t-test).

promoted the accumulation of p24 in the cell, as measured by western blotting and CBA (Fig. 5A,E,G), resulting in decreased viral release to the supernatant (Fig. 5F).

We next examined the VCCs of macrophages infected with HIV-1 GAG-iGFP-ΔENV-VSVG for 4 days and treated for additional 4 days with PF396 (Fig. 5H). Although PF396 had no evident impact on the macrophage morphology, including cell volume (Fig. 5I), it led to a significant increase in the compartment volume (from 42.26 µm^3 in DMSO-treated cells to 103.13 µm^3 in PF396-treated cells) (Fig. 5J), without an impact on the mean intensity of the Gag–iGFP signal (Fig. 5K). These VCCs from PF396-treated MDMs often had a granular or reticulated appearance (Fig. 5H; Fig. S5A). Although F-actin remained localized close to the compartment in PF396-treated cells, it appeared evenly distributed throughout the VCC, rather than being concentrated as patches in one side, as commonly observed in vehicle-treated cells (Fig. 5H). Despite their larger volume, VCCs from PF396-treated cells were more compact, as revealed by their decreased spreading scores (Fig. 5L). Although CD18 remained enriched in the vicinity of the VCC after PF396 treatment, its distribution was more even, as observed with F-actin (Fig. 5M; Fig. S5A). Shorter treatments with PF396 (24 h) caused a trend towards larger VCC and decreased spreading scores, although without statistical significance (Fig. S5B–F), possibly due to the large heterogeneity of the compartment and the fact that the drug does not act synchronously in all cells, as observed with jasplakinolide. To circumvent this limitation, we live-imaged HIV-1 Gag–iGFP-infected MDMs immediately after PF396 treatment, to follow the same cell overtime (Fig. S5G; Movie 3). These experiments confirmed the progressive accumulation of the compartment in perinuclear regions and that this occurs over multiple days.

Owing to the increased compactness of VCC from PF396-treated macrophages, we hypothesized that the VCC continuity with the plasma membrane might be altered after exposure to the drug, which could explain the decreased viral particle release. We thus exposed PF396-treated or vehicle-treated macrophages to CellBrite®, a non-permeable lipophilic dye that can withstand fixation. Strikingly, we observed strong accumulation of the dye in VCCs from DMSO-treated macrophages, whereas those from PF396-treated cells were generally negative for CellBrite staining (Fig. 5N–P). PYK2 is known for its critical role in regulating actin dynamics at focal adhesions (Schaller, 2010). Our data suggest that it is endowed with a similar role at the VCC, promoting its trafficking to the surface and regulating its connectivity to the plasma membrane.

Frustrated phagocytosis of HIV-1-infected MDMs induces the rapid release of viral particles from the VCC

Although our previous experiments have examined the role of the actin cytoskeleton in regulating HIV release from resting macrophages, we aimed to observe its impact in cells undergoing a dynamic process. For that, we subjected HIV-1-infected MDMs to frustrated phagocytosis. In this experimental system, macrophages spread rapidly on the substrate, driven by actin polymerization that promotes a fast and concentric extension of pseudopods, until the plasma membrane tension increases to a point that no longer allows further spreading (Masters et al., 2013). If an HIV-1-infected macrophage is subjected to frustrated phagocytosis, we hypothesized that the VCC could act as a membrane reservoir that could be deployed rapidly to the surface to counteract the increase in plasma membrane tension, and that their anchoring to the cytoskeleton would be required for such rapid deployment. We thus seeded MDMs, infected for 3 days with HIV-1-GAG-iGFP-ΔENV-VSVG, over a human IgG-coated surface and performed live imaging. As exemplified in Fig. 6A, the macrophage spread rapidly on the surface with its projected area more than doubling in 20 min (Fig. 6A, B; Movie 4). We further observed a steady decrease in the volume of the VCC starting at ∼8 min (Fig. 6A,B). The compartment appears to migrate towards the basal surface, as the cell spreads, where its intensity decreases, presumably due to virion release (Fig. 6A, xz planes). Indeed, by quantifying the amount of p24 in the culture supernatant, we observed a rapid release of the capsid protein from MDMs seeded over IgG-coated coverslips as compared with control coverslips or control coverslips with IgG added at the same time as the cells ('Soluble IgG'; Fig. 6C), during the first 2 h. Such rapid kinetics suggests that it is the preformed viral particles stored in VCCs that are released during frustrated phagocytosis and not a general increase in viral production due to macrophage activation. Supporting this idea, at later timepoints, there were no differences in the concentration of p24 released from macrophages seeded in the three conditions (Fig. 6C). Thus, as macrophages spread during frustrated phagocytosis, VCCs appear to be pulled to the basal surface of the cell, where they release their contents.

We next tested whether the actin cytoskeleton participates in VCC trafficking during frustrated phagocytosis. We fixed

Journal of Cell Science (2022) 135, jcs260511. doi:10.1242/jcs.260511

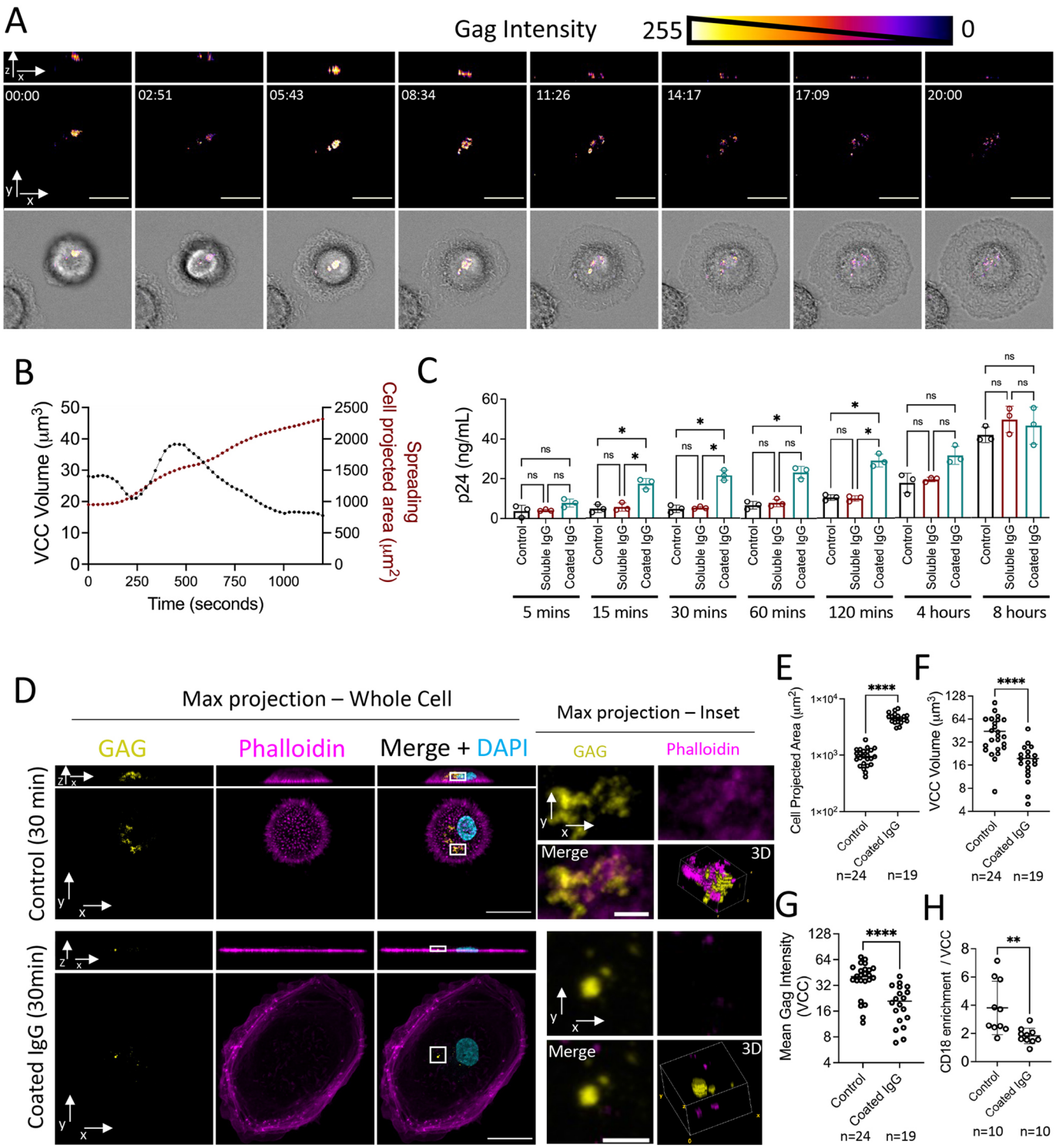

Fig. 6. Rapid HIV release during macrophage frustrated phagocytosis is associated with trafficking of CD18⁺ VCC to the surface. (A) Time-lapse imaging of MDMs infected with HIV-1-GAG-iGFP-ΔENV-VSVG for 3 days and seeded over human IgG-coats coverslips. Whole-cell projections are shown for the top and middle panels, along the *z*-axis (middle) or the *y*-axis (top). The bottom panel (transmission channel) is a single *z*-slice. Times shown are in minutes and seconds. Scale bars: 20 µm. (B) Image analysis of the total VCC volume (left *y*-axis) and the cell projected area (right *y*-axis) over the course of the frustrated phagocytosis event depicted in A. Result for A,B are representative of experiments with two independent donors. (C) MDMs infected with HIV-1-ΔENV-VSVG for 3 days were seeded over human IgG-coated coverslips, or over non-coated coverslips, or in the presence of soluble IgG over non-coated coverslips. At the indicated timepoints, aliquots of the supernatant were recovered and the released p24 was quantified by CBA. Data from three independent donors (mean±s.d.). **P*<0.05; ns, not significant (each timepoint group was compared by one-way ANOVA with Dunnett's multiple comparisons test). (D) Confocal microscopy of MDMs infected with HIV-1-Gag-iGFP-ΔENV-VSVG (MOI=1.0) for 3 days and seeded over control or human IgG-coated coverslips for 30 mins. Left panels show whole-cell projections along the *z*-axis (bottom) or the *y*-axis (top). Magnifications of the areas enclosed in the dashed squares are shown as z-projections on the right. Scale bars: 20 µm (left panels), 2 µm (right panels). (E–H) Image analysis for cells processed as in D for the indicated parameters. See Materials and Methods for details on the quantification strategies employed. Each circle represents one cell, and the plots include cells from two independent donors (mean values indicated by horizontal lines, with error bars showing s.d. in H). ***P*<0.01; *****P*<0.0001 (unpaired two-tailed *t*-test.).

Journal of Cell Science

Journal of Cell Science (2022) 135, jcs260511. doi:10.1242/jcs.260511

HIV-1-infected MDMs subjected to frustrated phagocytosis or in control conditions, and examined them by confocal microscopy (Fig. 6D). In cells under frustrated phagocytosis, F-actin concentrated on the protruding edges and as expected, these cells spread over the glass surface (Fig. 6E). The VCCs were significantly reduced in their volume in cells undergoing frustrated phagocytosis (Fig. 6F), as was the mean intensity of the Gag–iGFP signal (Fig. 6G). Interestingly, the remaining VCCs in MDMs under frustrated phagocytosis were mostly devoid of associated F-actin (Fig. 6D). Furthermore, whereas VCCs from control MDMs were associated with CD18, as expected, after frustrated phagocytosis the remaining VCCs lost this association (Fig. 6H; Fig. S6A). Finally, P-PYK2 (Y402) concentrated mostly in the protruding edges in cells under frustrated phagocytosis, whereas the remaining VCC in general lacked P-PYK2 (Fig. S6B). This strongly suggests that the rapid deployment of the VCCs to the surface that occurs during frustrated phagocytosis, requires an associated cytoskeleton and focal adhesion-like coats, and that compartments lacking such associated complexes remain inside the macrophage after frustrated phagocytosis.

DISCUSSION

Overall, our data highlights the importance of the actin cytoskeleton and associated factors in regulating the release of HIV-1 from its VCC in macrophages, likely by providing a physical anchor that promotes its movement, connectivity with the plasma membrane and, consequentially, viral release. Although previous studies had addressed the presence of an actin cytoskeleton associated with the VCC or IPMC, and its importance for viral release, the molecular details remained unknown. Here, we uncover an important role for the CD18–PYK2 axis as a modulator of the VCC structure, its trafficking dynamics and viral release.

By exposing infected MDMs to different pharmacologic modulators of the cytoskeleton, we found that the F-actin-stabilizing drug jasplakinolide significantly impacted viral release to the supernatant. A previous report demonstrated an increase in viral release from HIV-1-infected macrophages after treatment with the actin-depolymerizing drug latrunculin or the actin polymerization inhibitors cytochalasin E or D (Mlcochova et al., 2013). In our hands, the actin-depolymerizing drug mycalolide B had no significant effect on viral release over a 24-h period. Differences in the viral strains employed, experimental conditions or the distinct mechanisms through which mycalolide B and latrunculin depolymerize actin (Hayashi-Takanaka et al., 2019) might account for the divergent results. Although both drugs induced rounding up of the macrophage, only jasplakinolide had significant effects on the properties of the VCC during a 24-h exposure. Longer time exposure to these drugs is likely to induce artefacts or strong toxic effects, and thus we chose jasplakinolide as an effective compound to manipulate the actin cytoskeleton and explore its effects on the VCC.

The ARP2/3 complex inhibitor CK666 had no effect in viral release over 24 h. Longer exposure to CK666 led to toxic effects, so we cannot exclude that in the long-term actin polymerization might be required for viral release. Nevertheless, at least in the short term, actin polymerization might not be necessary for HIV release from macrophages. Similarly, the myosin II inhibitor blebbistatin had no significant effect on viral release over a 24-h period, suggesting that actomyosin contraction is not a major driver of viral release, at the steady state.

The use of pharmacological manipulation of the actin cytoskeleton is not without its shortcomings, due to its critical importance in multiple other biological processes. During HIV infection actin impacts virtually on every step of the viral cycle (Ospina Stella and Turville, 2018). To minimize 'off-target' effects, we allowed the establishment of the infection and formation of VCCs for 4 days before addition of the cytoskeleton modulators, so as to exclude any effect on the early steps of the viral cycle. Nevertheless, we cannot dismiss the possibility that certain unwanted effects might indirectly impact on HIV release.

Jasplakinolide treatment had no effect on p24 release from infected HeLa cells. Previous work has shown that although latrunculin augments viral release from macrophages, it has no effect on infected HEK 293 cells (Mlcochova et al., 2013). Given that, in these cell lines, HIV-1 viral particles directly bud to the extracellular medium, their release might not be impacted by modulating actin dynamics. Nevertheless, studies addressing the impact of viral release from non-macrophage cells have often yielded inconsistent results (Ospina Stella and Turville, 2018). Some reports suggest that actin might be important for the assembly and budding processes (Thomas et al., 2015; Wen et al., 2014), but this is at odds with a study that tracked individual budding sites in real-time in HeLa cells, demonstrating that assembly and budding proceeded unimpaired even after total depolymerization of actin (Rahman et al., 2014). Thus, it will be important to standardize experimental approaches to study the effects of the actin cytoskeleton on HIV assembly and budding. In macrophages, the field will face the added challenge of discriminating between the impact of actin modulation on viral assembly and budding, and its influence on VCC trafficking, as both might impact on viral release.

In HIV-infected macrophages exposed to jasplakinolide, VCCs scattered throughout the cell and were smaller, but more numerous, such that their total volume increased. They were devoid of associated actin, CD18 and the focal adhesion-like coats typically found in non-treated infected cells. In non-treated and infected macrophages, we observed that actin bundles frequently radiated from these VCC coats, suggesting that they are the site of anchoring of the cytoskeleton to the compartment. Jasplakinolide induces the loss of these structures, concomitant with the fragmentation of the compartment, suggesting an important role for the coats and their associated cytoskeleton in maintaining the integrity of the VCC, and potentially in promoting the fusion of smaller compartments into larger ones or inhibiting the fission of larger compartments.

Our frustrated phagocytosis assays indicate an important role for the actin cytoskeleton and VCC-associated CD18 in the trafficking of the compartment to the surface. We show that the drastic remodelling of the macrophage morphology that occurs in frustrated phagocytosis leads to rapid viral release, associated with loss of VCCs. Importantly, those VCCs remaining in the cell after frustrated phagocytosis were small and mostly devoid of actin and CD18, suggesting that these are required for rapid VCC trafficking to the surface and viral release. VCCs appear to be pulled rapidly to the basal surface of the cell during frustrated phagocytosis. Is the pulling force transmitted through the actin bundles connected to the compartment, as our observations suggest? If yes, where does such force originate from, and what is the role of the electron-dense coats that surround the VCC? One can speculate that the coats act as traction points, upon which pulling forces might act, in a manner akin to focal adhesions during mesenchymal cell migration (Bear and Haugh, 2014). In this scenario, one would expect a role for actomyosin contraction at the origin of the pulling forces acting on the VCC. Although we failed to observe any effect of myosin II inhibition in viral release from macrophages at the steady state, its impact might be more prominent during an event such as frustrated

Journal of Cell Science (2022) 135, jcs260511. doi:10.1242/jcs.260511

phagocytosis, where VCCs rapidly traffic through the cell. However, given the known role for myosin II in the formation of phagocytic cups, we could not test the impact of its inhibition in viral release during frustrated phagocytosis (Olazabal et al., 2002). Future studies, employing alternative approaches able to specifically isolate the role of myosin II in VCC trafficking could help answer this question.

We found that the phosphorylated form of the kinase PYK2 localizes at the VCC, and that jasplakinolide treatment redistributes it throughout the cell. The key role this kinase plays in regulating the dynamics of focal adhesions in macrophages, prompted us to explore its importance in HIV release. Inhibiting PYK2 led to viral particle accumulation in the macrophage, associated with larger VCCs that often had a granular appearance. Although F-actin and CD18 associated with the VCC via patches or focal points in control cells, treatment with the PYK2 inhibitor led to a more even distribution of these factors on the compartment. This suggests that PYK2 inhibition leads to altered organization of the focal adhesion-like coats that attach the actin cytoskeleton to the VCC, which might underlie its impact on viral release. PYK2 inhibition also led VCCs to lose plasma membrane connectivity, concomitant with the increased compaction of the compartment and perinuclear location. In vehicle-treated and infected cells, certain VCC were connected to the plasma membrane, whereas others where not, in agreement with previous observations (Deneka et al., 2007; Gaudin et al., 2013). In bone marrow macrophages from ‘humanized’ mice infected with HIV-1, completely enclosed compartments are often perceived, and these occasionally fused with plasma membrane-connected compartments (Ladinsky et al., 2019). Integrating these observations with our new data, VCCs appear to alternate between enclosed and plasma membrane-connected states, in a manner regulated by PYK2 activity. These enclosed compartments maintain the expression of classical VCC markers, such as CD18 and CD44, despite remaining inaccessible to antibodies added prior to cell fixation and permeabilization.

PYK2 phosphorylation has been previously reported during HIV-1 infection and occurs downstream of co-receptor engagement by the envelope glycoprotein gp120 (Del Corno et al., 2001), but not when Δ*Env* pseudotyped viruses are used (Davis et al., 1997). Our results, in contrast, point to an upregulation of PYK2 after prolonged (4 days) HIV-1-Δ*Env* infection, with a comparable increase in the levels of P-PYK2 (Tyr-402). In macrophages, HIV can reprogramme cell migration, via its accessory protein Nef, towards a mesenchymal mode (Vérollet et al., 2015), which depends on adhesive structures such as podosomes (Van Goethem et al., 2010) and is associated with PYK2 activation (Duong and Rodan, 2000). It is thus possible that a later activation or upregulation of PYK2 via a Nef-dependent mechanism might contribute to enhancing viral release from macrophages.

A limitation of our study that could be explored in future research was the use of *Env*-deficient viruses pseudotyped with VSV-G to achieve single-cycle infections. This strategy avoids propagation of the infection, which could indirectly impact the quantification of viral release. However, in our cultures, direct viral transmission from one cell to another does not occur due to the absence of the viral envelope. VCCs are often observed in proximity to the viral synapse that forms between an infected and a target cell (Duncan et al., 2014; Gousset et al., 2008), where they potentially participate in direct viral transmission. Interestingly, direct transmission of HIV-1 from macrophages to $CD4^+$ T cells is inhibited by jasplakinolide (Duncan et al., 2014), suggesting that the same actin-dependent mechanisms that regulate VCC trafficking for viral release also impact its redistribution towards viral synapses. It would be valuable to explore whether the factors described in this work as regulating viral release and VCC trafficking, such as PYK2 or the VCC coats, also play a role in cell-to-cell HIV transmission.

To conclude, whether at the steady-state or upon a stimulus that requires sudden and drastic changes in macrophage morphology, VCCs appear to be dynamic structures that traffic through the cell in a manner that depends on its associated actin and microtubule cytoskeleton (Gaudin et al., 2012). In tissues, macrophages are constantly subjected to mechanical constraints as they navigate through crowded tissues, in a manner dependent on cytoskeletal dynamics. Our work suggests that HIV might exploit macrophage biology to promote its own release and propagation.

MATERIALS AND METHODS

Ethics statement

Plasmapheresis residues from healthy adult donors were obtained from the Établissement Français du Sang (Paris, France) in accordance with the Institut National de la Santé et de la Recherche Médicale (France) (INSERM) ethical guidelines. According to French Public Health Law (art L 1121–1-1, art L 1121–1-2), written consent and Institutional Review Board approval are not required for human noninterventional studies.

Cells

Peripheral blood mononuclear cells (PBMCs) were separated using Ficoll-Paque (GE Healthcare), and monocytes were isolated by positive selection using CD14+ magnetic beads (Miltenyi Biotec) and differentiated into macrophages for 7 days in RPMI (Gibco, Life Technologies) supplemented with 5% fetal calf serum (FCS; Gibco), 5% human serum AB (Sigma), 1% of 10,000 U/ml penicillin and 100 µg/ml of streptomycin (Gibco), and 25 ng/ml macrophage colony-stimulating factor (M-CSF; Miltenyi Biotec).

HeLa (CRM-CCL-2™, ATCC) and HEK 293 FT (R70007, Thermo Fisher Scientific) cells were maintained by bi-weekly subpassage in DMEM (Gibco, Thermofisher Scientific), supplemented with 10% FCS and 1% of 10,000 U/ml of penicillin and 100 µg/ml of streptomycin. Cells lines are routinely authenticated and screened for mycoplasma contamination.

Virus production and monocyte transduction with LifeAct–mCherry

Viral particles were produced by transfection of 293FT cells in six-well plates with 3 µg of total DNA and 8 ml TransIT-293 Transfection Reagent (Mirus Bio) per well. Plasmid mixes to produce HIV-1 viral particles consisted of 0.4 µg CMV-VSVG (pMD2.G; Addgene 12259) and 2.6 µg of HIV proviral plasmid. To quantify viral release we preferentially used viral particles produced from pNL-ΔENV-VSVG which was kindly provided by Olivier Schwartz (Institut Pasteur, Paris, France). For examination of the VCC by microscopy we employed the pNL-GAG-iGFP-ΔENV-VSVG, a viral construct in which EGFP is placed between viral protease cleaving sites and between the matrix and capsid domains of Gag (Hubner et al., 2007). In other experiments, we also employed an infectious viral clone pNL-AD8. Medium was renewed 16 h later, and viruses were harvested at around 48 h after transfection, filtered through a 0.45 µm pore and stored at −80°C until use. Thawed viral stocks were titrated by infecting the GHOST X4R5 reporter cell line.

A similar protocol was followed to produce lentiviral particles for monocyte transduction with Lifeact–mCherry. Here, transfection mixes consisted of 0.4 µg CMV-VSVG, 1.0 µg of the packaging plasmid PSPAX2 (Addgene 12260) and 1.6 µg of LifeAct–mCherry lentivector (pCDH1-CMV-LifeAct-mCherry). In parallel, VPX-containing SIV particles were produced by transfecting 293FT cells with 0.4 µg CMV-VSVG and 2.6 µg of $pSIV3^+$ plasmid (Mangeot et al., 2000). Monocytes were transduced with equal volumes of freshly harvested LifeAct–mCherry and SIV3 lentiviral particles in the presence of 8 µg/ml of protamine (Sigma). At 48 h, differentiating MDMs were exposed to 2 µg/ml of puromycin to select for successfully transduced cells, and were harvested for experiments at day 7 of differentiation.

Journal of Cell Science (2022) 135, jcs260511. doi:10.1242/jcs.260511

In vitro infections and cell treatments

MDMs were infected with HIV-1 NL-GAG-iGFP-ΔENV-VSVG, NL-ΔENV-VSVG or NL-AD8-VSVG at the MOIs indicated in the figures or figure legends. After 16 h, culture medium was renewed, and the infection allowed to progress for a further 72 h. When employing the fully infectious clone NL-AD8, fusion inhibitors (maraviroc, 5 µM and T20, 5 µM) were added at the moment of culture medium renewal to block propagation of the infection after the first round. At day 4 after infection, cells were exposed to the drugs or vehicle (DMSO) at concentrations and for the time periods indicated in figure legends [jasplakinolide (Sigma); CK666 (Sigma); blebbistatin (Sigma); mycalolide B (Enzo Life Sciences); PF431396 (Tocris)].

HeLa cells were infected with NL-ΔENV-VSVG at a MOI=1.0. After 16 h, the culture medium was renewed, and the same drugs added at similar concentrations.

To assess the membrane connectivity of the VCC, we employed the CellBrite Fix membrane stain. Briefly, infected MDMs were rinsed in PBS and incubated for 15 min at 37°C with a 1:1000 dilution of CellBrite Fix-640 (Biotium). Cells were rinsed twice with PBS and fixed in 4% paraformaldehyde (PFA) for confocal microscopy.

To assess the accessibility of VCC to anti-CD44 antibodies, infected MDMs were rinsed in PBS and stained with anti-CD44 antibodies at room temperature for 15 mins, before rinsing twice with PBS and fixation with PFA 4%. Cells were subsequently processed for confocal microscopy as described below.

Frustrated phagocytosis

Glass coverslips (12 mm) were extensively washed with 70% ethanol, dried and incubated with 10 µg/ml of IgG from human serum (Sigma) in PBS for 1 h at room temperature. For quantification of p24 release, 24-well culture plates were directly coated with human IgG. MDMs were infected with HIV-1 NL-GAG-iGFP-ΔENV-VSVG for microscopy, or with HIV-1 NL-ΔENV-VSVG for p24 quantification at a MOI=1.0. At day 3 after infection, cells were detached, washed and seeded over IgG-coated substrates (5000 cells for microscopy, 20,000 for p24 quantification). Cells were subsequently fixed in PFA at 30 mins for fixed cell confocal microscopy, or immediately imaged for live-cell imaging. For p24 release quantification, aliquots of the supernatant were collected at the indicated time-points, filtered (0.45 µm) to remove floating cells, and stored until quantification with the p24 CBA.

Quantification of p24 in culture supernatant or cell lysates by cytometric bead array

Culture supernatant or cell pellets were lysed in a buffer containing 0.1% BSA, 1% NP-40 and 0.02% Tween-20. The amount of p24 in samples was subsequently quantified by a custom-made CBA assay that detects the HIV-1 p24 protein. Briefly, B6 functional beads (BD Biosciences) were conjugated with an anti-GAG antibody (H183-H12-5C hybridoma (mouse IgG1), NIH) and serve as capturing beads by incubation with samples for 1 h at room temperature with agitation. An anti-p24 detection antibody (KC57-FITC, Beckmann Coulter) is subsequently added and incubated for 2 h at room temperature. After two washes in a buffer containing 0.1% NP-40, beads are flowed in a FACS Verse (BD Biosciences) and the p24 concentration in culture estimated using a standard curve with serial dilutions of recombinant p24. For cell lysates, an aliquot of the sample was used to quantify total protein by the BCA method (Pierce Micro BCA kit, Thermo Fisher Scientific) and the data is presented as µg of p24/mg of total cell protein.

Validation of the cytometric bead assay for p24

To confirm that our CBA assay specifically detects the p24 capsid protein and not the full length p55 Gag, we transfected HEK 293FT cells grown in six-well plates with 3 µg of pNL-ΔEnv. After 18 h, medium was renewed and a range of concentrations of saquinavir (indicated in Fig. S2A–C). After a further 24 h, medium was harvested and filtered (0.45 µm). An aliquot (50 µl) was employed to quantify p24 by CBA and the rest was ultracentrifuged (40,000 ***g***, 2 h) over a sucrose gradient of 20%. Pelleted viral particles were lysed in RIPA buffer and analysed by western blot to obtain the Gag processing profiles. In other experiments, viruses were produced in HEK 293 FT cells in the presence of 5 µM of saquinavir and supernatant aliquots were recovered at the time points indicated in Fig. S2D, and p24 was quantified by CBA.

Western blotting

Cells were lysed in RIPA buffer and total protein levels quantified with the BCA method. 30 µg of sample was reduced with Laemmli buffer, boiled and loaded in pre-cast polyacrylamide gels (Bio-Rad). After transfer onto PDVF membranes (Bio-Rad), blocking buffer [5% non-fat dry milk (w/v) in PBS-Tween-20 0.1% (v/v)] was added for 1 h at room temperature. Primary antibodies were added overnight at 4°C with gentle agitation in antibody dilution buffer (5% BSA in PBS containing 0.1% Tween-20), washed and incubated with species-matched secondary HRP-conjugated secondary antibodies for 1 h at room temperature. Membranes were revealed in a Bio-Rad Chemidoc after addition of HRP substrate (Clarity, Bio-Rad). Densitometry quantifications were performed using the ImageLab software (Bio-Rad). Uncropped images of western blots from this study are shown in Fig. S7.

Confocal microscopy and immunostaining

Cells were fixed in 4% PFA, washed in PBS and then permeabilized with permeabilization buffer [1% BSA (w/v) and 0.3% Triton X-100 (v/v) in PBS] for 1 h at room temperature. The primary antibodies used were anti-F-actin, anti-CD18, anti-pPYK2 and anti-CD44, as listed in Table S1. Primary antibodies were diluted in permeabilization buffer, and the staining was performed overnight at 4°C in the dark. Subsequently, cells were washed 3 times and secondary staining was done in permeabilization buffer supplemented with 5% Donkey serum (Sigma) for 1 h. For secondary antibodies, donkey anti-rabbit-IgG Alexa Fluor 647 or donkey anti-mouse-IgG Alexa Fluor 647 (Invitrogen) were used. Phalloidin–AF647 (Invitrogen) staining was also performed at this stage. Cells were washed three times then rinsed in PBS and mounted in Fluoromont-GTM medium with DAPI (Invitrogen).

Cell imaging was performed on an inverted confocal microscope (Leica DMi8, SP8 scanning head unit) equipped with a 63× oil immersion objective (NA=1.4) and four laser diodes (405, 488, 546 and 633 nm). An optimized *z*-step of 0.31 µm was employed for all acquisitions.

Image analysis and quantification

ImageJ was used for all image analyses and quantifications, using custom-made macro scripts to automate the analysis, which can be provided upon contacting the corresponding authors. The Gag–iGFP signal was used to define a binary mask on the VCC, at each *z*-slice. Then, we sum the intensities of the binary mask across the *z*-axis, at each *x,y* pixel. The resulting image will provide a projection of the VCC in the *x,y* plane while also preserving the quantitative information in the *z*-axis. This is then adjusted for the scale of the image to obtain the volume of the VCC. A similar strategy was employed to estimate the total cell volume. Depending on the staining, the binary masks to define the cell area at each *z*-slice were derived from the phalloidin, F-actin or CD18 staining. Mean Gag intensity corresponds to the average Gag–iGFP signal at the region defined as the VCC by the binary mask.

To calculate VCC dispersion (spreading) across the cell, we used maximum intensity projections of the VCC binary mask and determined its centroid. Spreading was then determined by calculating the average distance of each VCC pixel in the projected mask to the centroid. A similar strategy was used to calculate the average distance of the VCC from the nucleus centroid. In this case, DAPI was used to define the nuclear binary mask, which after maximum intensity projection, was used to determine its centroid.

To determine the enrichment of CD18, P-PYK2 or CellBrite at the VCC, we first defined the VCC and cell binary masks and obtained the average intensity for the CD18, P-PYK2 or CellBrite staining in both the VCC and the whole cell. The enrichment score was then obtained as the ratio between the average intensity at the VCC and the average intensity in the whole cell.

All image montages were assembled using ImageJ. *y*-projections were obtained using the Reslice tool, followed by maximum intensity projections. The 3D reconstructions were achieved by applying the Volume Viewer plugin to the binary masks of the channels imaged.

Live-cell imaging

For live imaging experiments, cells were imaged on an inverted confocal microscope (Leica DMi8, SP8 scanning head unit) equipped with a 40× oil immersion objective and a live-cell imaging chamber to maintain a constant temperature of 37°C and CO2 levels of 5%.

To assess the dynamics of the actin cytoskeleton surrounding the VCC, MDMs transduced with LifeAct–mCherry were infected with HIV-1 GAG-iGFP ΔENV-VSVG at a MOI=1.0 for 6 days in glass bottom 35-mm dishes (Ibidi). *z*-stacks were acquired in real-time at a frame rate of 0.42/s.

To image infected MDMs during frustrated phagocytosis, cells were placed in the imaging chamber immediately after their addition to IgG-coated 35-mm glass bottom disks. *z*-stacks were acquired at a frame rate of 0.041/s. Acquired images were processed in ImageJ to assemble videos and montages.

To evaluate the impact of jasplakinolide or PF396 on the VCC by live imaging, we employed an Incucyte S3 system, which allows long-term imaging of cells in culture. In brief, MDMs were infected with HIV-1 Gag-iGFP-ΔEnv-VSVG for 4 days. Medium was renewed and jasplakinolide (100 nM), PF396 (1.0 µM) or vehicle (DMSO) were added, and cells placed in the Incucyte and imaging was started. For the experiments with jasplakinolide, and due to the rapid effects of the drug, an image was taken every 30 min. In the case of experiments with PF396, an image was taken every 2 h. Binary masks for the VCC were obtained using the Incucyte analysis software. Images were cropped and movies prepared using ImageJ.

Electron microscopy

MDMs infected with HIV-1-NL-ΔENV-VSVG, were fixed in 2% glutaraldehyde in 0.1 M cacodylate buffer, pH 7.4 for 1 h and subsequently fixed for 1 h in 2% buffered osmium tetroxide, dehydrated in a graded series of ethanol solution, and then embedded in epoxy resin. Images were acquired with a digital camera Quemesa (SIS) mounted on a Tecnai Spirit transmission electron microscope (FEI) operated at 80 kV.

Statistical analysis

Data were analysed using Prism software v9 (GraphPad). If not specified in figure legends, graphics show individual donors as dots with bars or lines at the means. Distributions were assumed to be non-parametric, and the specific test employed is indicated at the figure legend. ns, *P*-value of >0.05; *$P \leq 0.05$; **$P \leq 0.01$; ***$P \leq 0.001$; ****$P \leq 0.0001$.

Acknowledgements

We thank Dr Claire Hivroz and Ana-Maria Lennon-Dumenil at Institut Curie for fruitful discussions and critical reading of the manuscript. We also thank François-Xavier Gobert and Nicolas Carpi for discussions or technical help.

Competing interests

The authors declare no competing or financial interests.

Author contributions

Conceptualization: V.R., M.M., P.B.; Methodology: V.R., S.T., M.S.-R., E.G., A.H.; Validation: V.R., P.B.; Formal analysis: V.R., S.T.; Investigation: V.R., S.T., M.S.-R., E.G., A.H.; Resources: M.M.; Data curation: V.R.; Writing - original draft: V.R., S.T., P.B.; Writing - review & editing: V.R., M.M., M.S.-R., P.B.; Supervision: V.R., P.B.; Funding acquisition: P.B.

Funding

This work was supported by grants from Agence Nationale de Recherche contre le SIDA et les hépatites virales (ANRS), Ensemble contre le SIDA (Sidaction), Laboratoire d'Excellence (Labex) DCBIOL (ANR-10-IDEX-0001-02 PSL and ANR-11-LABX-0043) to P.B. V.R. was supported by fellowships from ANRS and Sidaction.

Peer review history

The peer review history is available online at https://journals.biologists.com/jcs/lookup/doi/10.1242/jcs.260511.reviewer-comments.pdf.

References

Bear, J. E. and Haugh, J. M. (2014). Directed migration of mesenchymal cells: where signaling and the cytoskeleton meet. *Curr. Opin. Cell Biol.* **30**, 74-82. doi:10.1016/j.ceb.2014.06.005

Berre, S., Gaudin, R., Cunha de Alencar, B., Desdouits, M., Chabaud, M., Naffakh, N., Rabaza-Gairi, M., Gobert, F. X., Jouve, M. and Benaroch, P. (2013). CD36-specific antibodies block release of HIV-1 from infected primary macrophages and its transmission to T cells. *J. Exp. Med.* **210**, 2523-2538. doi:10.1084/jem.20130566

Chu, H., Wang, J. J., Qi, M., Yoon, J. J., Wen, X., Chen, X., Ding, L. and Spearman, P. (2012). The intracellular virus-containing compartments in primary human macrophages are largely inaccessible to antibodies and small molecules. *PLoS One* **7**, e35297. doi:10.1371/journal.pone.0035297

Davis, C. B., Dikic, I., Unutmaz, D., Hill, C. M., Arthos, J., Siani, M. A., Thompson, D. A., Schlessinger, J. and Littman, D. R. (1997). Signal transduction due to HIV-1 envelope interactions with chemokine receptors CXCR4 or CCR5. *J. Exp. Med.* **186**, 1793-1798. doi:10.1084/jem.186.10.1793

Del Corno, M., Liu, Q. H., Schols, D., de Clercq, E., Gessani, S., Freedman, B. D. and Collman, R. G. (2001). HIV-1 gp120 and chemokine activation of Pyk2 and mitogen-activated protein kinases in primary macrophages mediated by calcium-dependent, pertussis toxin-insensitive chemokine receptor signaling. *Blood* **98**, 2909-2916. doi:10.1182/blood.V98.10.2909

Deneka, M., Pelchen-Matthews, A., Byland, R., Ruiz-Mateos, E. and Marsh, M. (2007). In macrophages, HIV-1 assembles into an intracellular plasma membrane domain containing the tetraspanins CD81, CD9, and CD53. *J. Cell Biol.* **177**, 329-341. doi:10.1083/jcb.200609050

Duncan, C. J., Williams, J. P., Schiffner, T., Gärtner, K., Ochsenbauer, C., Kappes, J., Russell, R. A., Frater, J. and Sattentau, Q. J. (2014). High-multiplicity HIV-1 infection and neutralizing antibody evasion mediated by the macrophage-T cell virological synapse. *J. Virol.* **88**, 2025-2034. doi:10.1128/JVI.03245-13

Duong, L. T. and Rodan, G. A. (2000). PYK2 is an adhesion kinase in macrophages, localized in podosomes and activated by β2-integrin ligation. *Cell Motil. Cytoskeleton* **47**, 174-188. doi:10.1002/1097-0169(200011)47:3<174::AID-CM2>3.0.CO;2-N

Gaudin, R., de Alencar, B. C., Jouve, M., Berre, S., Le Bouder, E., Schindler, M., Varthaman, A., Gobert, F. X. and Benaroch, P. (2012). Critical role for the kinesin KIF3A in the HIV life cycle in primary human macrophages. *J. Cell Biol.* **199**, 467-479. doi:10.1083/jcb.201201144

Gaudin, R., Berre, S., Cunha de Alencar, B., Decalf, J., Schindler, M., Gobert, F. X., Jouve, M. and Benaroch, P. (2013). Dynamics of HIV-containing compartments in macrophages reveal sequestration of virions and transient surface connections. *PLoS One* **8**, e69450. doi:10.1371/journal.pone.0069450

Gousset, K., Ablan, S. D., Coren, L. V., Ono, A., Soheilian, F., Nagashima, K., Ott, D. E. and Freed, E. O. (2008). Real-time visualization of HIV-1 GAG trafficking in infected macrophages. *PLoS Pathog.* **4**, e1000015. doi:10.1371/journal.ppat.1000015

Graziano, F., Desdouits, M., Garzetti, L., Podini, P., Alfano, M., Rubartelli, A., Furlan, R., Benaroch, P. and Poli, G. (2015). Extracellular ATP induces the rapid release of HIV-1 from virus containing compartments of human macrophages. *Proc. Natl. Acad. Sci. USA* **112**, E3265-E3273. doi:10.1073/pnas.1500656112

Han, S., Mistry, A., Chang, J. S., Cunningham, D., Griffor, M., Bonnette, P. C., Wang, H., Chrunyk, B. A., Aspnes, G. E., Walker, D. P. et al. (2009). Structural characterization of proline-rich tyrosine kinase 2 (PYK2) reveals a unique (DFG-out) conformation and enables inhibitor design. *J. Biol. Chem.* **284**, 13193-13201. doi:10.1074/jbc.M809038200

Hayashi-Takanaka, Y., Kina, Y., Nakamura, F., Yamazaki, S., Harata, M., Soest, R., Kimura, H. and Nakao, Y. (2019). Effect of mycalolides isolated from a marine sponge Mycale aff. nullarosette on actin in living cells. *Sci. Rep.* **9**, 7540. doi:10.1038/s41598-019-44036-2

Hubner, W., Chen, P., Del Portillo, A., Liu, Y., Gordon, R. E. and Chen, B. K. (2007). Sequence of human immunodeficiency virus type 1 (HIV-1) Gag localization and oligomerization monitored with live confocal imaging of a replication-competent, fluorescently tagged HIV-1. *J. Virol.* **81**, 12596-12607. doi:10.1128/JVI.01088-07

Ladinsky, M. S., Khamaikawin, W., Jung, Y., Lin, S., Lam, J., An, D. S., Bjorkman, P. J. and Kieffer, C. (2019). Mechanisms of virus dissemination in bone marrow of HIV-1-infected humanized BLT mice. *Elife* **8**, e46916. doi:10.7554/eLife.46916

Mangeot, P. E., Nègre, D., Dubois, B., Winter, A. J., Leissner, P., Mehtali, M., Kaiserlian, D., Cosset, F. L. and Darlix, J. L. (2000). Development of minimal lentivirus vectors derived from simian immunodeficiency virus (SIVmac251) and their use for gene transfer into human dendritic cells. *J. Virol.* **74**, 8307-8315. doi:10.1128/JVI.74.18.8307-8315.2000

Masters, T. A., Pontes, B., Viasnoff, V., Li, Y. and Gauthier, N. C. (2013). Plasma membrane tension orchestrates membrane trafficking, cytoskeletal remodeling, and biochemical signaling during phagocytosis. *Proc. Natl. Acad. Sci. USA* **110**, 11875-11880. doi:10.1073/pnas.1301766110

Mlcochova, P., Pelchen-Matthews, A. and Marsh, M. (2013). Organization and regulation of intracellular plasma membrane-connected HIV-1 assembly compartments in macrophages. *BMC Biol.* **11**, 89. doi:10.1186/1741-7007-11-89

Okigaki, M., Davis, C., Falasca, M., Harroch, S., Felsenfeld, D. P., Sheetz, M. P. and Schlessinger, J. (2003). Pyk2 regulates multiple signaling events crucial for

macrophage morphology and migration. *Proc. Natl. Acad. Sci. USA* **100**, 10740-10745. doi:10.1073/pnas.1834348100

Olazabal, I. M., Caron, E., May, R. C., Schilling, K., Knecht, D. A. and Machesky, L. M. (2002). Rho-kinase and myosin-II control phagocytic cup formation during CR, but not FcγR, phagocytosis. *Curr. Biol.* **12**, 1413-1418. doi:10.1016/S0960-9822(02)01069-2

Orenstein, J. M., Meltzer, M. S., Phipps, T. and Gendelman, H. E. (1988). Cytoplasmic assembly and accumulation of human immunodeficiency virus types 1 and 2 in recombinant human colony-stimulating factor-1-treated human monocytes: an ultrastructural study. *J. Virol.* **62**, 2578-2586. doi:10.1128/jvi.62.8.2578-2586.1988

Ospina Stella, A. and Turville, S. (2018). All-round manipulation of the actin cytoskeleton by HIV. *Viruses* **10**, 63. doi:10.3390/v10020063

Pelchen-Matthews, A., Giese, S., Mlčochová, P., Turner, J. and Marsh, M. (2012). β2 integrin adhesion complexes maintain the integrity of HIV-1 assembly compartments in primary macrophages. *Traffic* **13**, 273-291. doi:10.1111/j.1600-0854.2011.01306.x

Rahman, S. A., Koch, P., Weichsel, J., Godinez, W. J., Schwarz, U., Rohr, K., Lamb, D. C., Krausslich, H. G. and Müller, B. (2014). Investigating the role of F-actin in human immunodeficiency virus assembly by live-cell microscopy. *J. Virol.* **88**, 7904-7914. doi:10.1128/JVI.00431-14

Rodrigues, V., Ruffin, N., San-Roman, M. and Benaroch, P. (2017). Myeloid cell interaction with HIV: a complex relationship. *Front. Immunol.* **8**, 1698. doi:10.3389/fimmu.2017.01698

Sattentau, Q. J. and Stevenson, M. (2016). Macrophages and HIV-1: an unhealthy constellation. *Cell Host Microbe* **19**, 304-310. doi:10.1016/j.chom.2016.02.013

Schaller, M. D. (2010). Cellular functions of FAK kinases: insight into molecular mechanisms and novel functions. *J. Cell Sci.* **123**, 1007-1013. doi:10.1242/jcs.045112

Thomas, A., Mariani-Floderer, C., López-Huertas, M. R., Gros, N., Hamard-Péron, E., Favard, C., Ohlmann, T., Alcamí, J. and Muriaux, D. (2015). Involvement of the Rac1-IRSp53-Wave2-Arp2/3 signaling pathway in HIV-1 gag particle release in CD4 T cells. *J. Virol.* **89**, 8162-8181. doi:10.1128/JVI.00469-15

Van Goethem, E., Poincloux, R., Gauffre, F., Maridonneau-Parini, I. and Le Cabec, V. (2010). Matrix architecture dictates three-dimensional migration modes of human macrophages: differential involvement of proteases and podosome-like structures. *J. Immunol.* **184**, 1049-1061. doi:10.4049/jimmunol.0902223

Vérollet, C., Souriant, S., Bonnaud, E., Jolicoeur, P., Raynaud-Messina, B., Kinnaer, C., Fourquaux, I., Imle, A., Benichou, S., Fackler, O. T. et al. (2015). HIV-1 reprograms the migration of macrophages. *Blood* **125**, 1611-1622. doi:10.1182/blood-2014-08-596775

Welsch, S., Keppler, O. T., Habermann, A., Allespach, I., Krijnse-Locker, J. and Kräusslich, H. G. (2007). HIV-1 buds predominantly at the plasma membrane of primary human macrophages. *PLoS Pathog.* **3**, e36. doi:10.1371/journal.ppat.0030036

Wen, X., Ding, L., Wang, J. J., Qi, M., Hammonds, J., Chu, H., Chen, X., Hunter, E. and Spearman, P. (2014). ROCK1 and LIM kinase modulate retrovirus particle release and cell-cell transmission events. *J. Virol.* **88**, 6906-6921. doi:10.1128/JVI.00023-14

Zhu, X., Bao, Y., Guo, Y. and Yang, W. (2018). Proline-rich protein tyrosine kinase 2 in inflammation and cancer. *Cancers* **10**, 139. doi:10.3390/cancers10050139

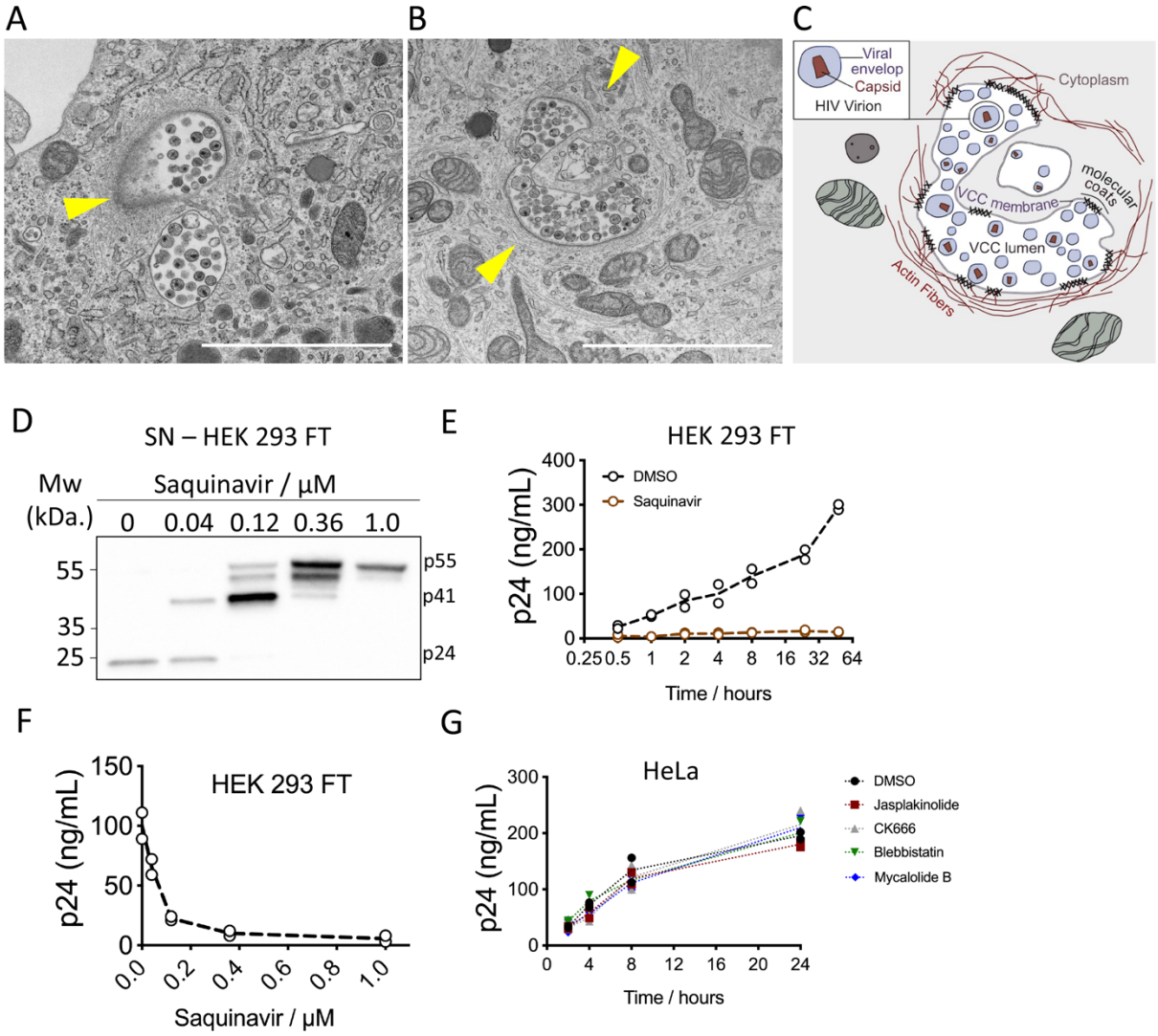

Fig. S1. Actin is tightly associated with VCC at the ultrastructural level. Validation of CBA assay and impact of actin modulation in HIV-1 release from HeLa cells

A-B – MDMs were infected with HIV-1-ΔENV-VSVG (MOI=1.0) for 7 days. Cells were fixed and processed for electron microscopy imaging. Arrowheads depict the VCC-associated actin cytoskeleton. Scale bar = 2 µm. Images from A and B are from two independent donors.

C – Cartoon depiction of S1B, highlighting the different structures associated with the VCC

D –Gag western blot from pelleted viral particles from HEK 293 FT cells transfected with pNL-ΔENV in the presence of the indicated concentrations of saquinavir. Data is from one representative experiment.

E – The same supernatants from S2A were filtered (0.45 µm) and p24 was quantified via a custom-made CBA assay. Data from one representative experiment. Each dot represents a technical replicate.

F – HEK 293FT cells were transfected with pNL-ΔENV-VSVG. After 16 hours, media was replaced, and cells were treated with the viral protease inhibitor Saquinavir (10 µM) or vehicle (DMSO). Supernatants were recovered at the indicated time-points, filtered (0.45 µm) and p24 quantified via a custom-made CBA assay. Data from one representative experiment. Each dot represents a technical replicate.

G – HeLa cells were infected with NL-ΔENV-VSVG (MOI=1.0). At 24 hours post-infection, culture media was replaced with fresh media containing the indicated inhibitors or vehicle (DMSO). Aliquots of the supernatant were recovered at the indicated time-points, filtered (0.45 µm) and p24 quantified by CBA. Jasplakinolide = 50 nM / CK666 = 10 µM / Blebbistatin = 5 µM / Mycalolide-B = 100 nM. Data from 3 independent experiments.

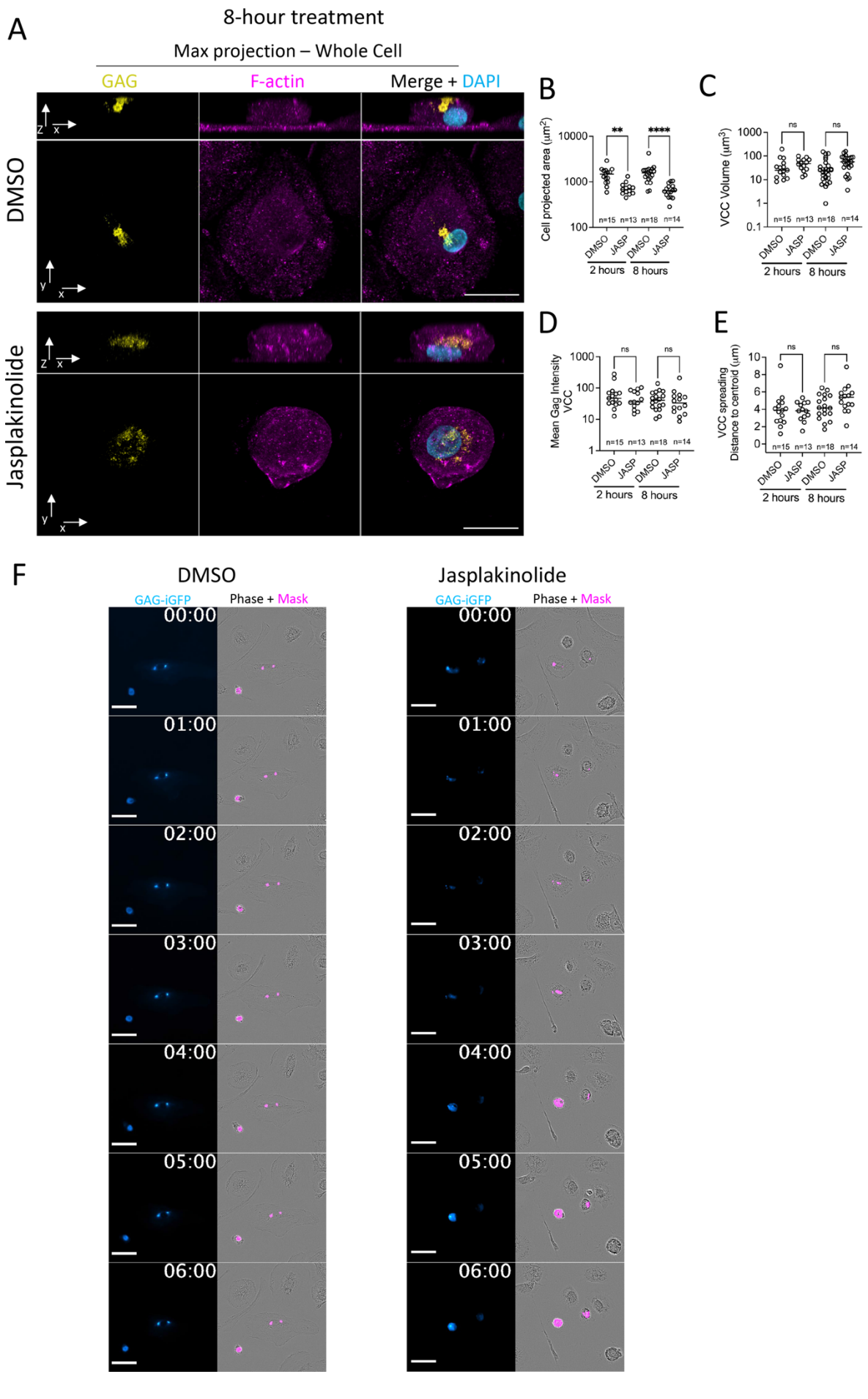

Fig. S2. Impact of shorter jasplakinolide treatment on the VCC

A - MDMs were grown in coverslips, infected with HIV-1-ΔENV-GAG-iGFP-VSVG at a MOI=1.0 for 4 days and subsequently treated with DMSO or jasplakinolide (100 nM) for 8 hours. Cells were fixed, stained with anti-F-actin and imaged by confocal microscopy. Whole-cell projections are shown along the z-axis (bottom) or the y-axis (top).

B-E- Image analysis for cells processed as in (A) for the indicated parameters. See methods for details on the quantification strategies employed. Each circle represents one cell and the plots display cells from 2 independent donors. Unpaired two-tailed t-test. (** = P<0.01; ****P<0.0001; ns-non-significant).

F - MDMs were grown in 24-well plates, infected with HIV-1-ΔENV-GAG-iGFP-VSVG at a MOI=1.0 for 4 days and subsequently treated with DMSO or jasplakinolide (100 nM). Cells were then placed in an Incucyte S3 and phase contrast and GFP images were acquired at a 30 min frequency. See also Movie 2. Time is in hours:minutes.

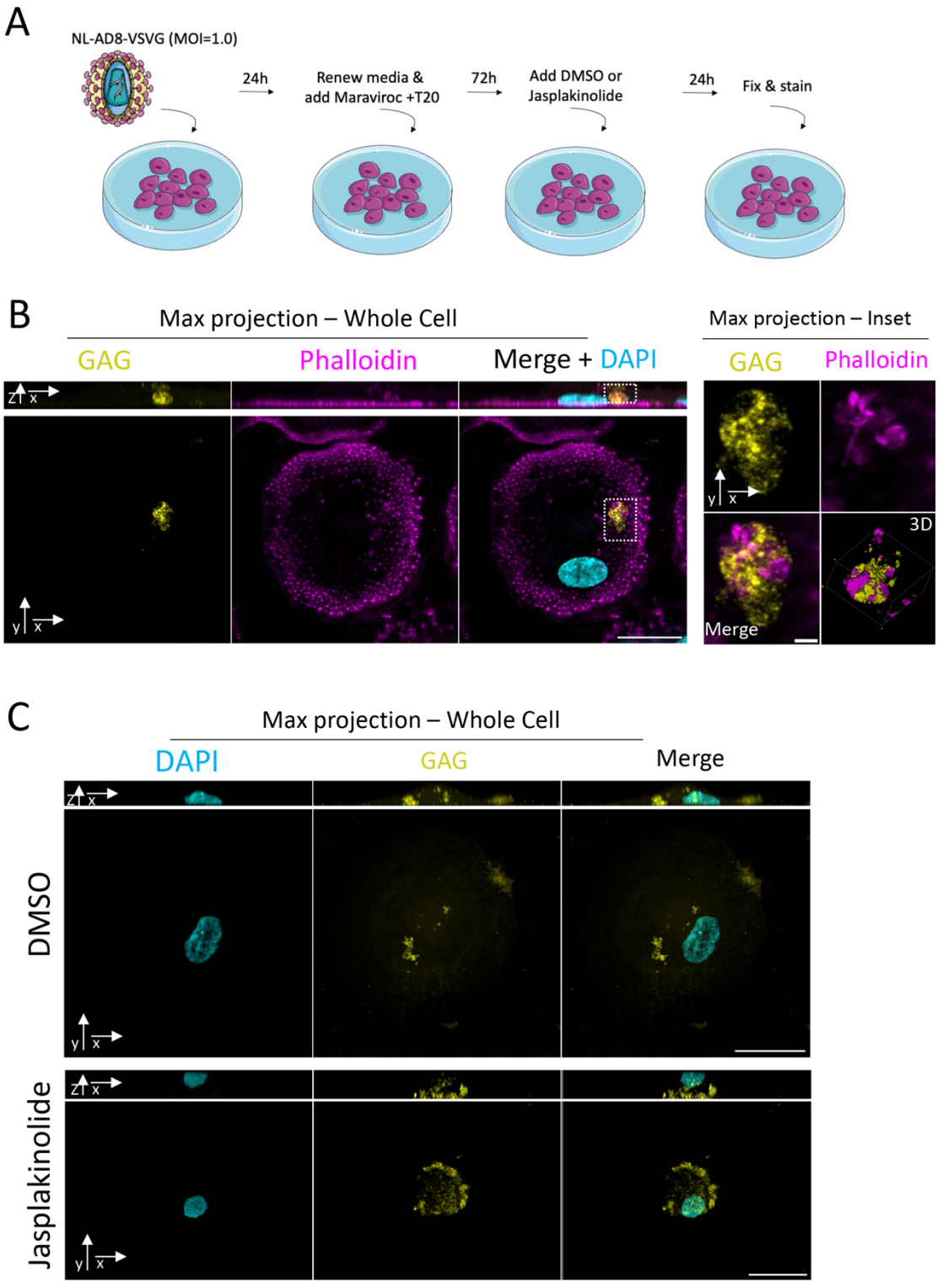

Fig. S3. Impact of actin cytoskeleton modulation in the VCC of MDMs infected with an infectious HIV-1 clone

A – Schematic representation of the experimental strategy to analyse the VCC in MDMs infected with an HIV-1 infectious clone. To prevent the propagation of the infection we added viral fusion inhibitors to the culture at 24 hours after the initial infection challenge.

B – Confocal microscopy of MDMs infected with HIV-1 NL-AD8-VSVG (MOI=1.0) for 6 days, in the presence of the viral fusion inhibitors, T20 and maraviroc, from day 2 onwards, and stained for GAG and Phalloidin. Whole cell projections are shown on the right, along the z-axis (bottom) or the y axis (top). On the left, the areas enclosed in the dashed squares are zoomed in and shown as z-projections. Scale bar = 20 µm (left panels) or 2 µm (right panels). Shown is a representative image from two independent donors.

C - Confocal microscopy of MDMs infected with HIV-1 NL-AD8-VSVG (MOI=1.0) for 4 days, in the presence of the viral fusion inhibitors, T20 and maraviroc, from day 2 onwards, and treated with DMSO (top panels) or jasplakinolide (bottom panels) for an additional 24 hours, before fixation and imaging of Gag-iGFP. Whole cell projections are shown, along the z-axis (bottom) or the y axis (top). Shown is a representative image from two independent donors.

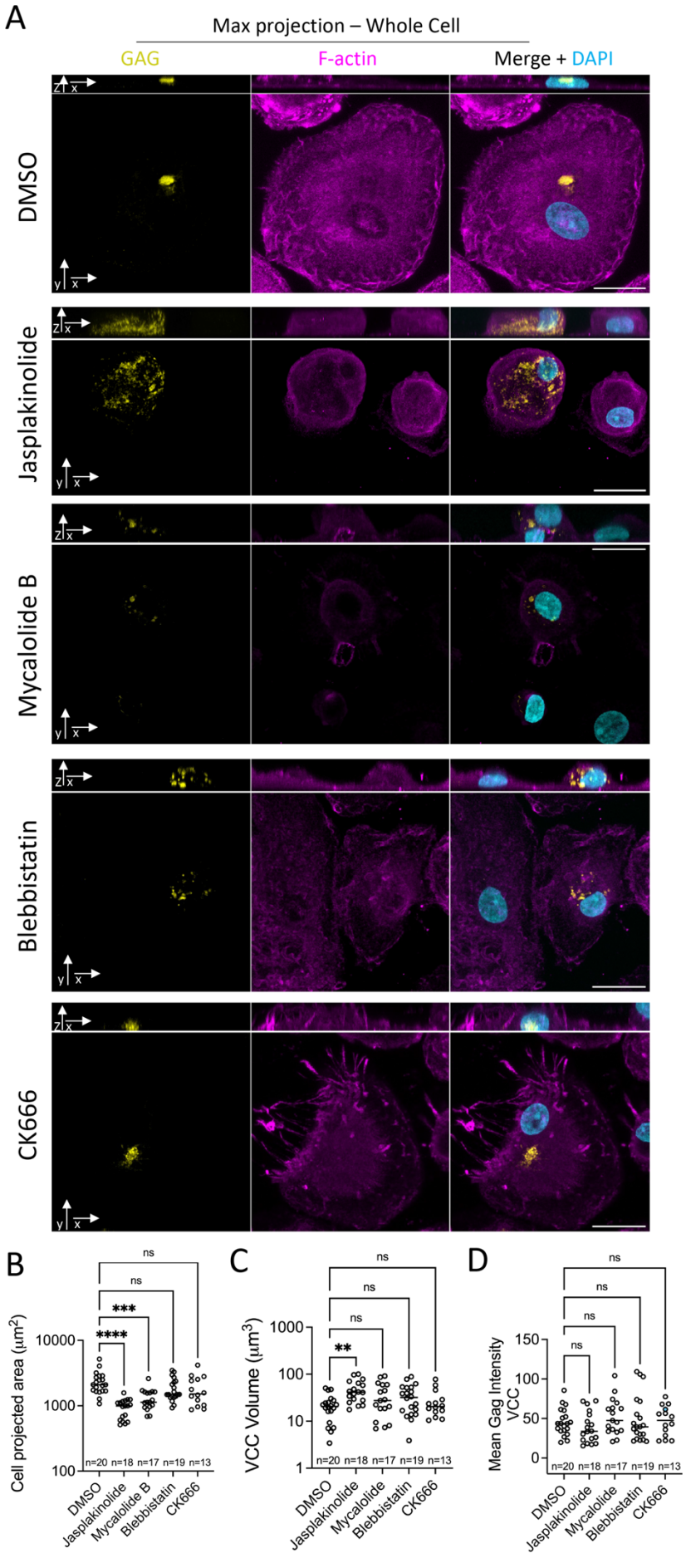

Fig. S4. Impact of cytoskeleton modulators on the properties of the VCC

A – Confocal microscopy of MDMs infected with HIV-1-Gag-iGFP-ΔENV-VSVG (MOI=1.0) for 4 days and treated with Jasplakinolide (50 nM), Mycalolide B (100 nM), Blebbistatin (5 μM), CK666 (10 μM) or vehicle (DMSO) for an additional 24 hours. Whole cell projections are shown, along the z-axis (bottom) or the y axis (top). Scale bar = 20 μm.

B – D - Image analysis for cells processed as in (A) for the indicated parameters. See methods for details on the quantification strategies employed. Each circle represents one cell, and the plots display cells from 2 independent donors. One-way ANOVA followed by Dunnett's multiple comparisons test. (** = $P<0.01$; **** $P<0.0001$; ns-non-significant).

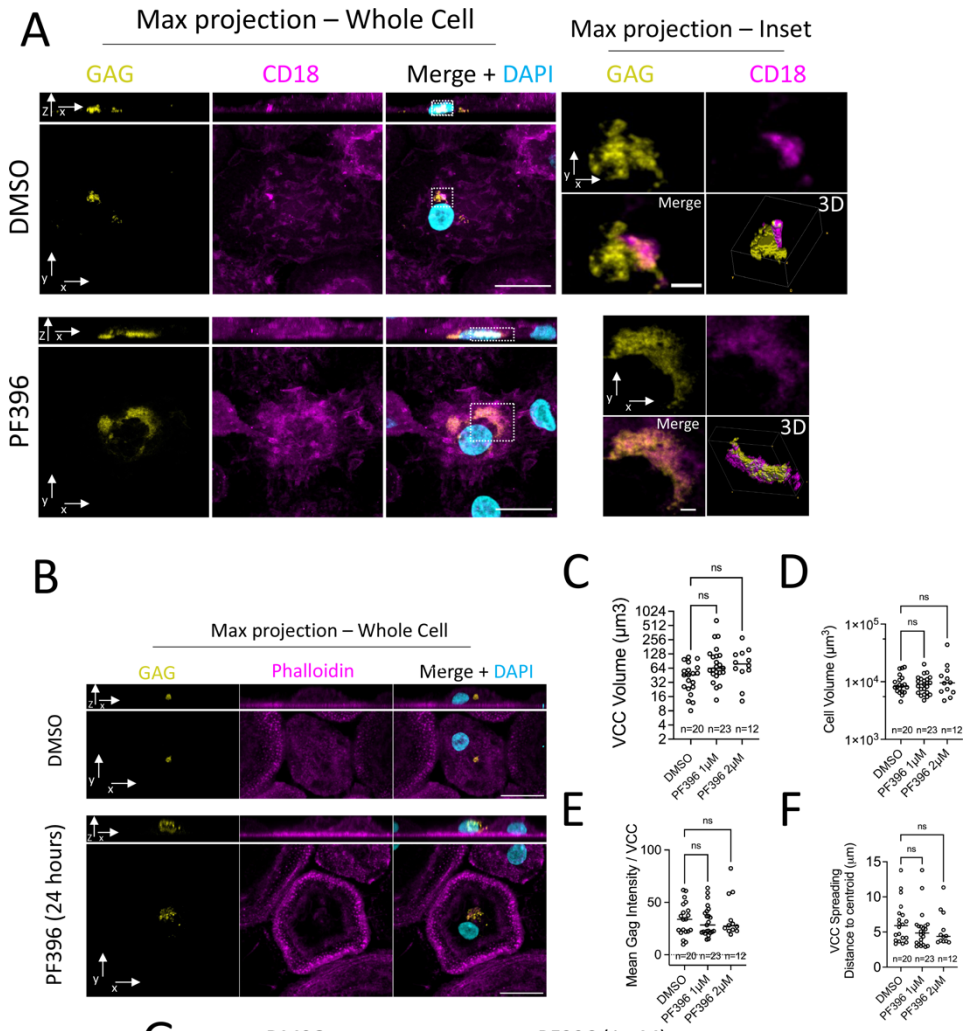

Fig. S5. Altered distribution of CD18 in VCC after PF396 treatment and effect of PF396 treatment on the VCC's characteristics at shorter time-points.

A – Confocal microscopy of MDMs infected with HIV-1-Gag-iGFP-ΔENV-VSVG (MOI=1.0) for 4 days and treated with PF396 (1μM) or vehicle (DMSO) for an additional 4 days. Whole cell projections are shown on the right, along the z-axis (bottom) or the y axis (top). On the left, the areas enclosed in the dashed squares are zoomed in and shown as z-projections. Scale bar = 20 μm (left panels) or 2 μm (right panels). Related to Figure 5M.

B - Confocal microscopy of MDMs infected with HIV-1-Gag-iGFP-ΔENV-VSVG (MOI=1.0) for 4 days and treated with PF396 (1 μM, bottom panels) or vehicle (DMSO, top panels) for an additional 24 hours. Whole cell projections are shown, along the z-axis (bottom) or the y axis (top). Scale bar = 20 μm.

C – F - Image analysis for cells processed as in (A) for the indicated parameters. See methods for details on the quantification strategies employed. Each circle represents one cell and the plots display cells from 2 independent donors. One-way ANOVA followed by Dunnett's multicomparisons test. (** = P<0.01; ****P<0.0001; ns-non-significant).

G - MDMs were grown in 24-well plates, infected with HIV-1-ΔENV-GAG-iGFP-VSVG at a MOI=1.0 for 4 days and subsequently treated with DMSO or PF396 (1 μM). Cells were then placed in an Incucyte S3 and phase contrast and GFP images were acquired at a 2-hour frequency.

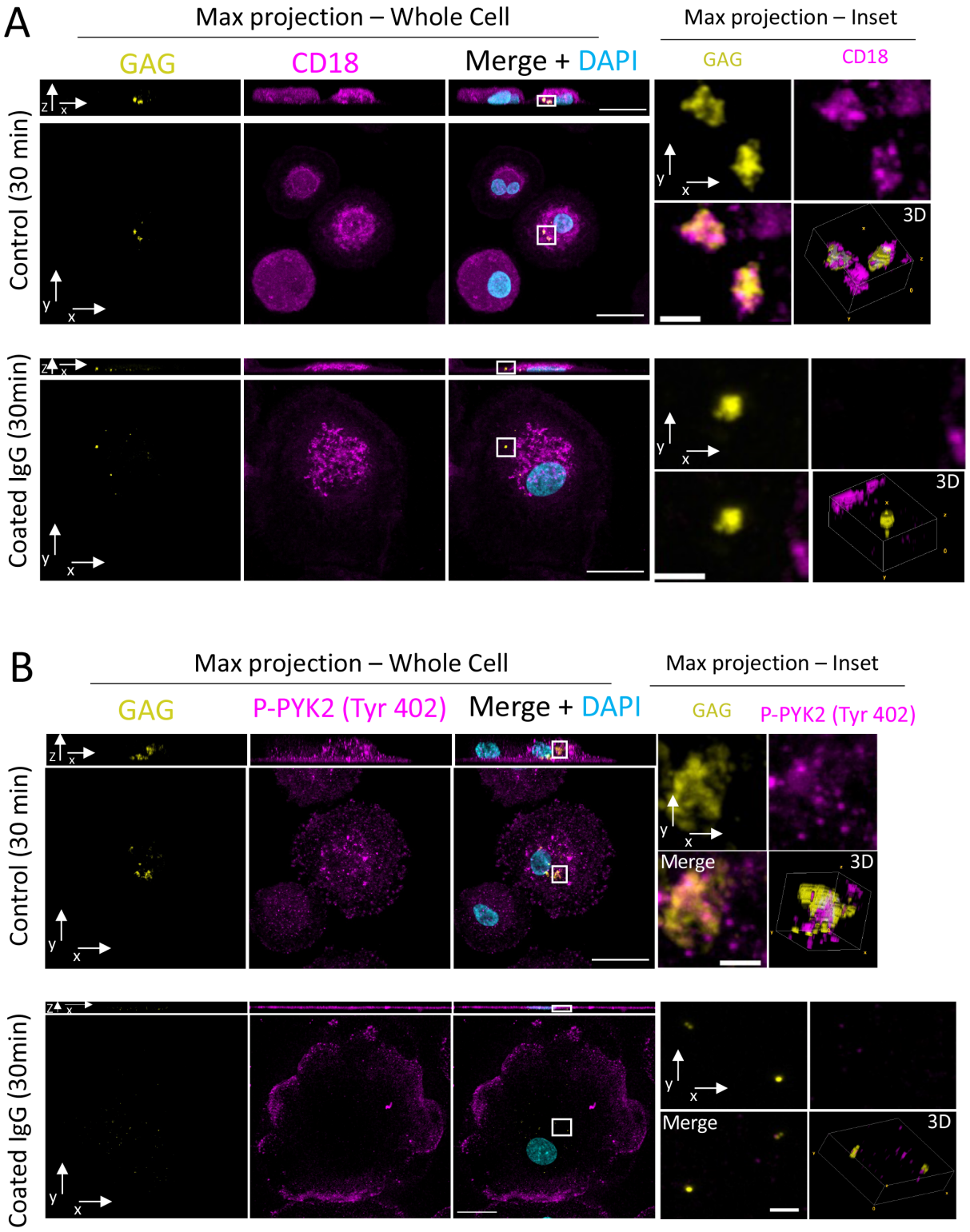

Fig. S6. CD18 and p-PYK2 localization at the VCC before and after frustrated phagocytosis

A-B – Confocal microscopy of MDMs infected with HIV-1-Gag-iGFP-ΔENV-VSVG (MOI=1.0) for 3 days and seeded over control or human IgG-coated coverslips for 30 mins. Right panels - whole cell projections along the z-axis (bottom) or the y axis (top). Left, panels – magnification of the areas enclosed in the dashed squares as z-projections. Scale bar = 20 µm (left panels) or 2 µm (right panels). Shown are representative examples from two independent donors.

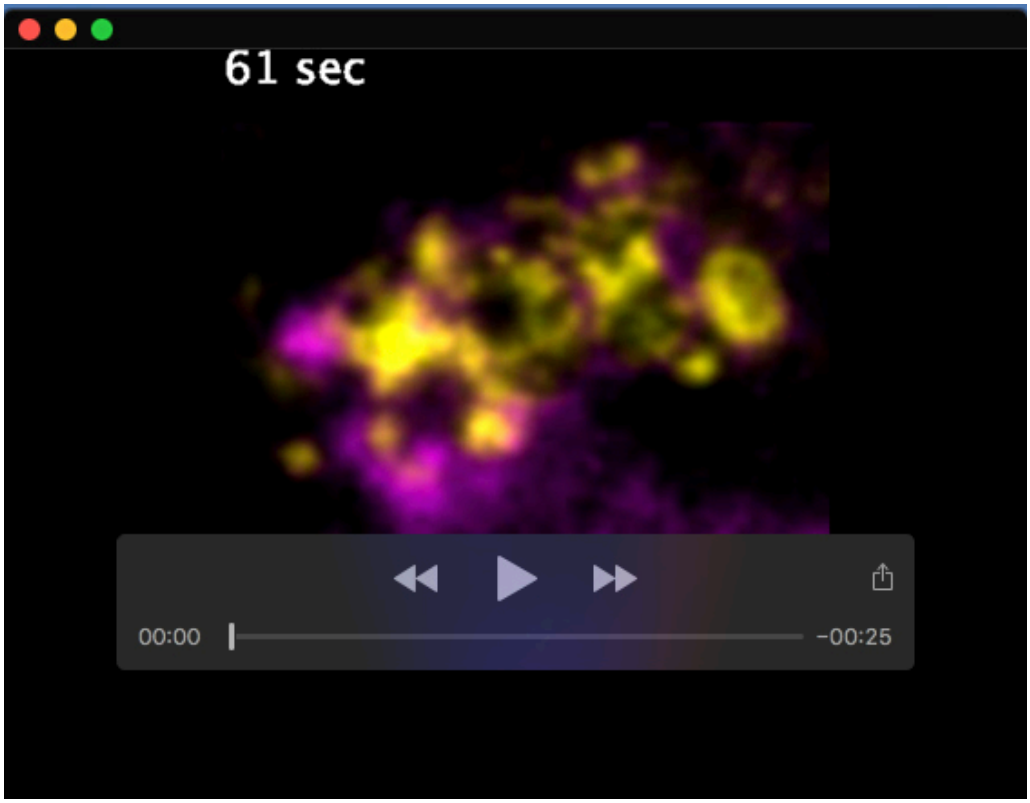

Movie 1. Dynamics of actin and VCC in HIV-1-infected macrophage

MDMs transduced with Lifeact-mCherry were infected with HIV-1-GAG-iGFP-ΔENV-VSVG (MOI=1.0). Time-lapse imaging was performed at day 6 after infection. Scale bar = 5 μm

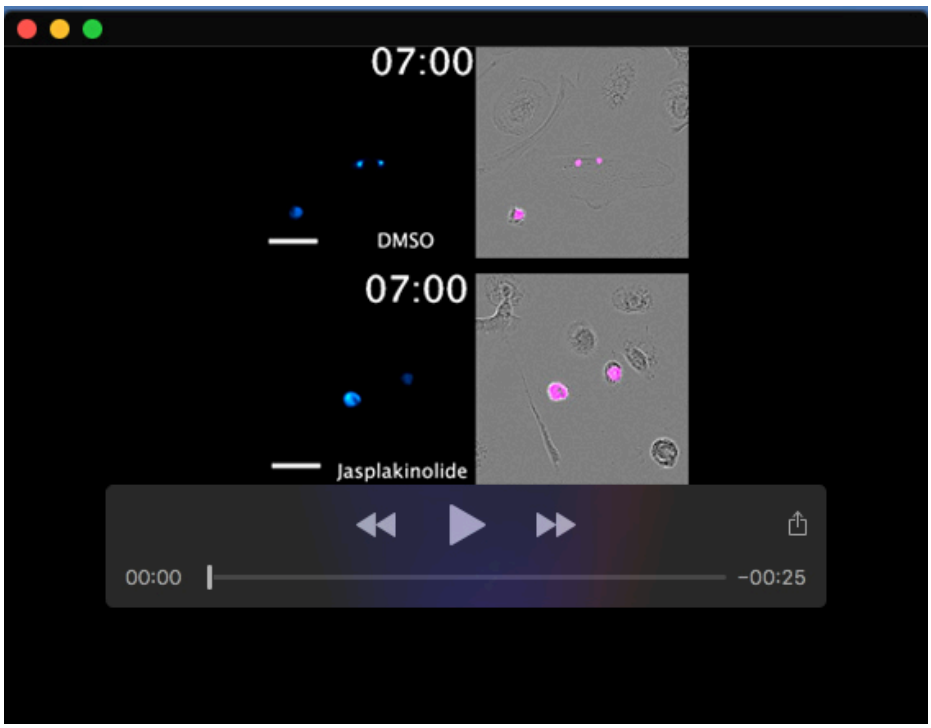

Movie 2. Dynamics of the VCC after jasplakinolide treatment

MDMs were grown in 24-well plates, infected with HIV-1-ΔENV-GAG-iGFP-VSVG at a MOI=1.0 for 4 days and subsequently treated with DMSO or jasplakinolide (100 nM). Cells were then placed in an Incucyte S3 and phase contrast and GFP images were acquired at a 30 min frequency.

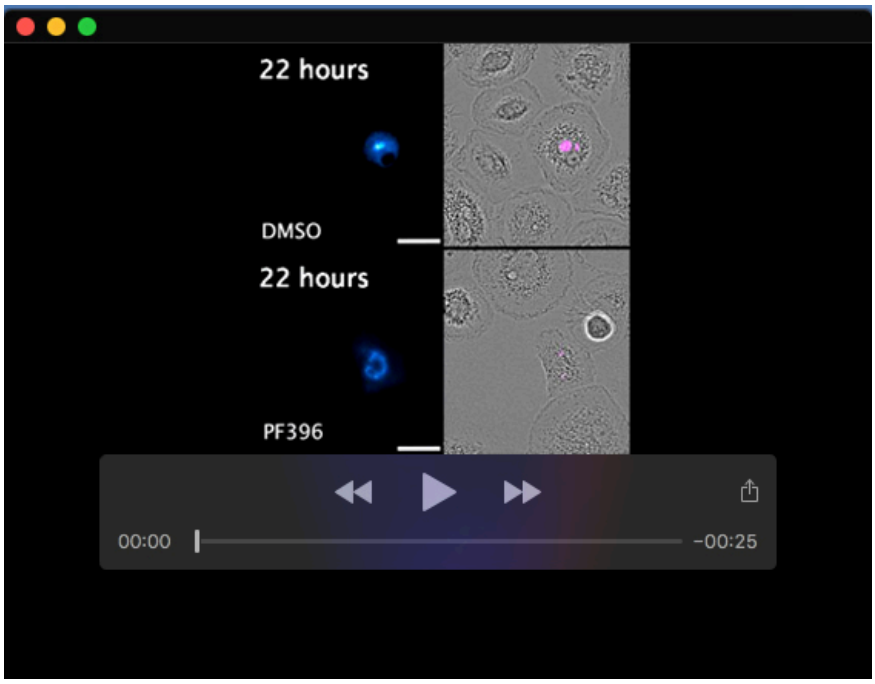

Movie 3. Dynamics of the VCC after PF396 treatment

MDMs were grown in 24-well plates, infected with HIV-1-ΔENV-GAG-iGFP-VSVG at a MOI=1.0 for 4 days and subsequently treated with DMSO or PF396 (1 μM). Cells were then placed in an Incucyte S3 and phase contrast and GFP images were acquired at a 2-hour frequency.

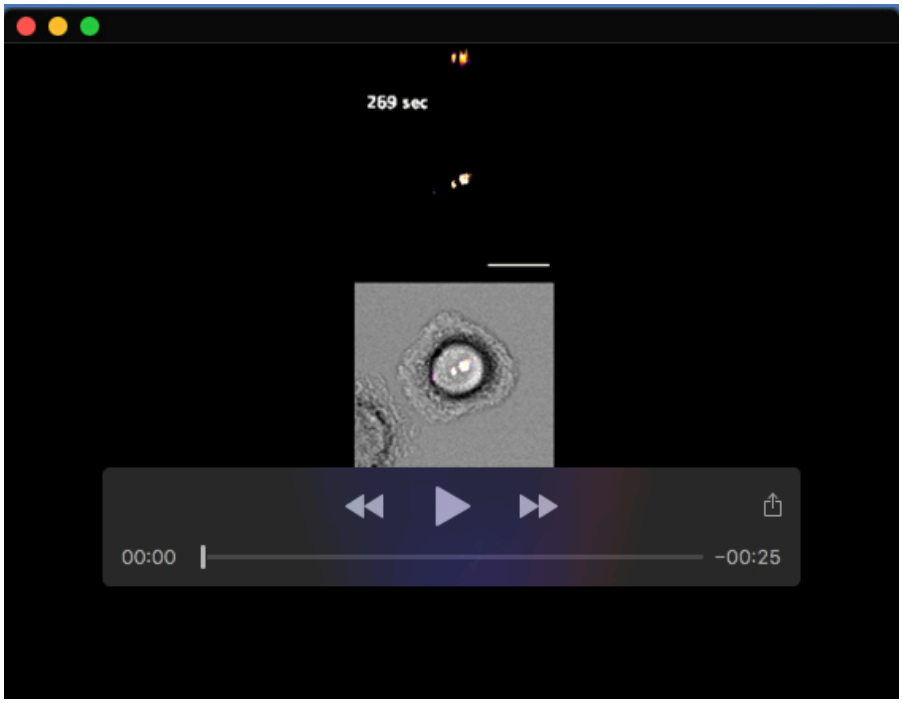

Movie 4. Live imaging of frustrated phagocytosis of HIV-1-infected macrophages.

Time-lapse imaging of MDMs infected with HIV-1-GAG-iGFP-ΔENV-VSVG for 3 days and seeded over human IgG-coats coverslips. Whole cell projections are shown for the top and middle panels, along the z-axis (middle) or the y axis (top). The bottom panel (transmission channel) is a single z-slice. Scale bar = 20 µm.

Table S1. Antibodies employed in this study

Antigen targeted	Application	Species	Dilution	Source	Reference / Validation
F-actin	Immunofluorescence	mouse	1/100	Abcam – ab205	(Wang *et al.*, 2020)
CD18	Immunofluorescence	mouse	1/100	Abcam – ab657	(Giese and Marsh, 2014)
p-PYK2 (TYR402)	Immunofluorescence/ Western blot	rabbit	1/100 (IF) 1/1000 (WB)	Abcam – ab4800	(Gunesch *et al.*, 2020)
CD44	Immunofluorescence	rat	1/100	BD - 550538	(Hagen *et al.*, 2018)
GAG	Western Blot	mouse	1/2000	NIH AIDS reagent resource - H183–H12–5C	(Gea-Mallorquí *et al.*, 2020)
GAPDH	Western blot	goat	1/2000	Abcam – ab157156	(Li *et al.*, 2020)
PYK2	Western Blot	rabbit	1/1000	Cell Signaling - 3292	(Tangeda *et al.*, 2022)
Anti-p24-FITC	CBA	mouse	1/200	Beckman Coulter / KC57	This article (Fig S2)

Fig. S7. Blot transparency

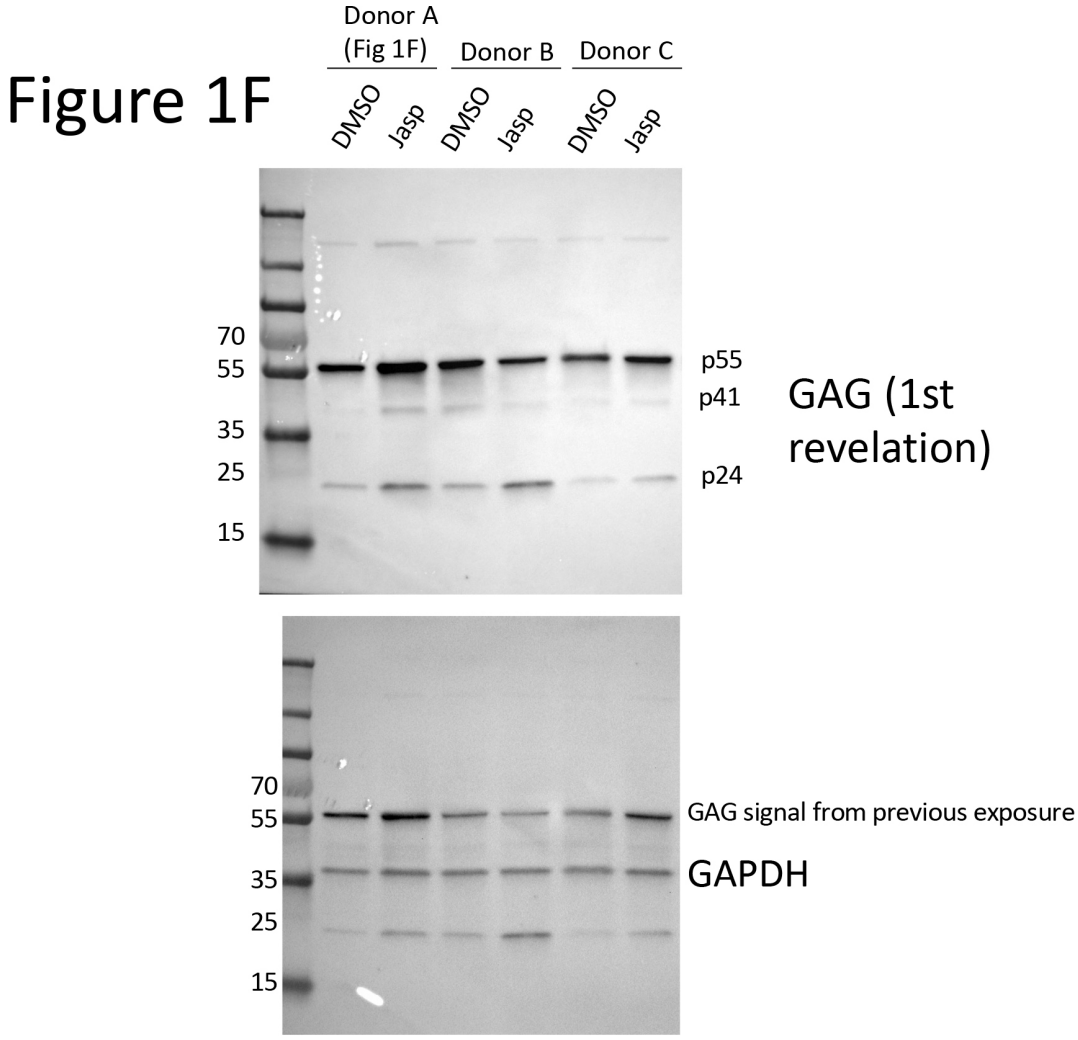

Figure 4D

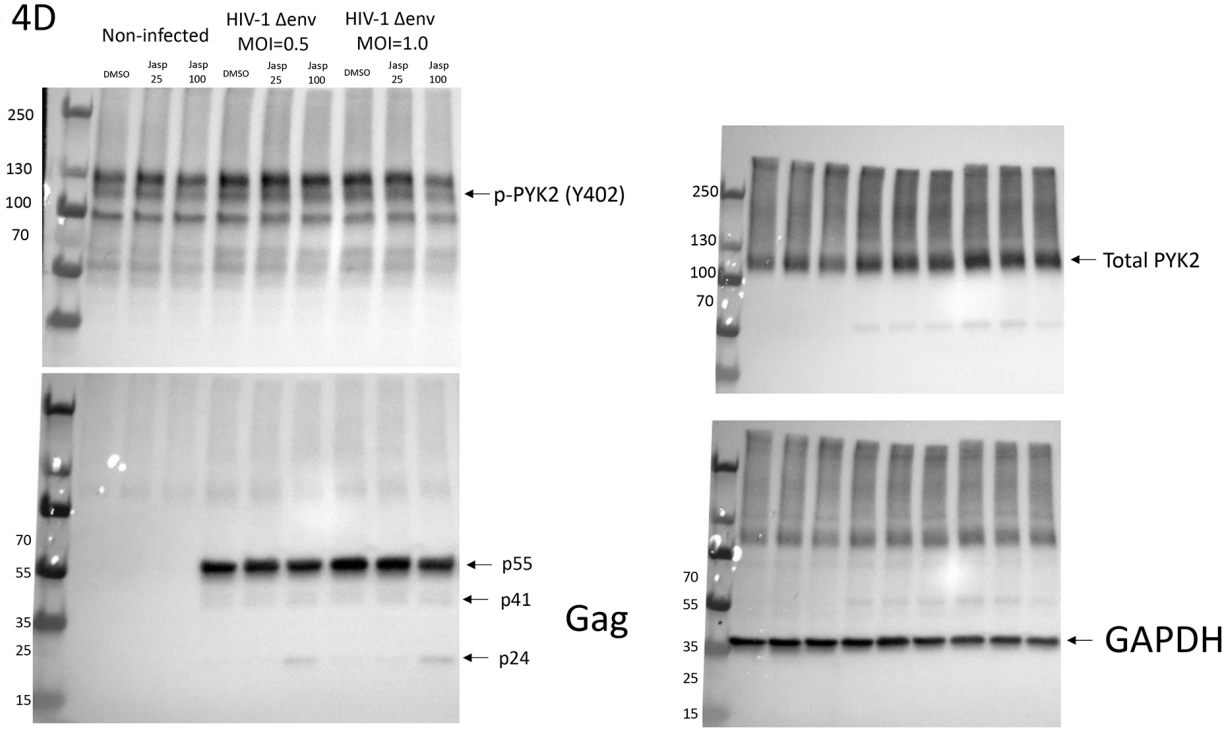

Figure 5A

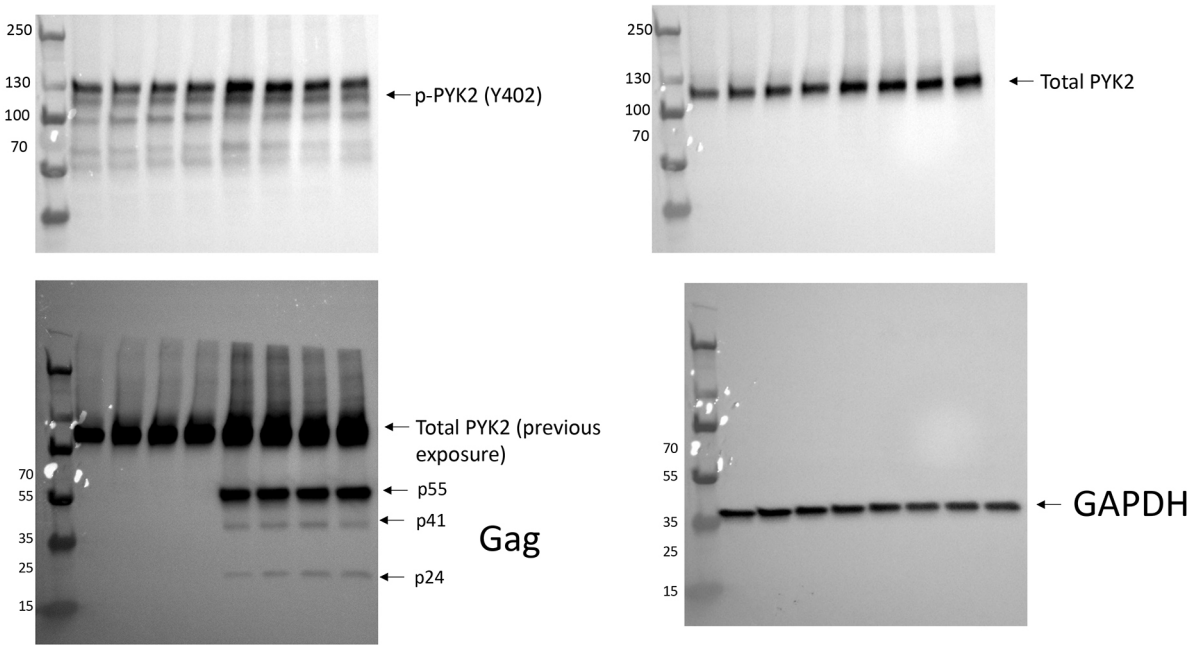

Figure S1D

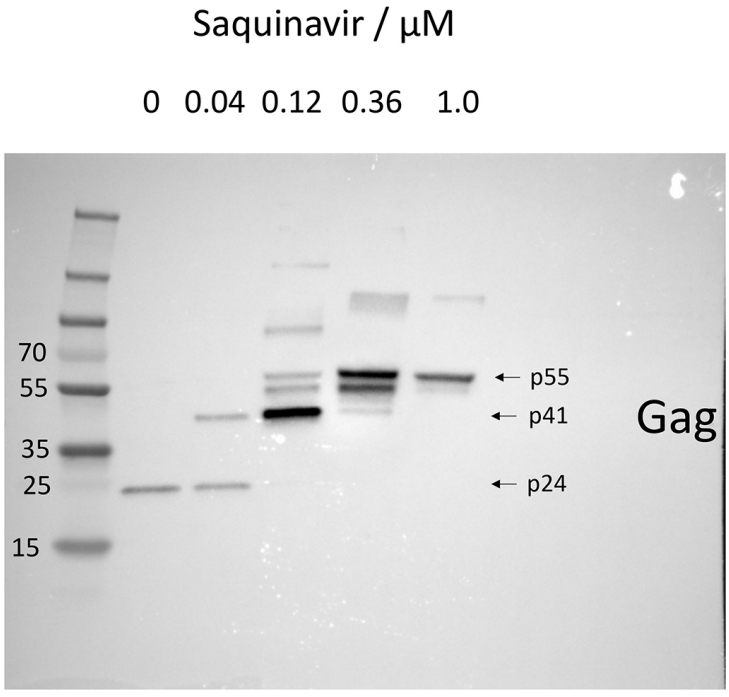

Supplementary References

Gea-Mallorquí, E. *et al.* (2020) 'HIV-2-Infected Macrophages Produce and Accumulate Poorly Infectious Viral Particles', *Frontiers in Microbiology*, 11, p. 1603. Available at: https://doi.org/10.3389/fmicb.2020.01603.

Giese, S. and Marsh, M. (2014) 'Tetherin can restrict cell-free and cell-cell transmission of HIV from primary macrophages to T cells', *PLoS pathogens*, 10(7), p. e1004189. Available at: https://doi.org/10.1371/journal.ppat.1004189.

Gunesch, J.T. *et al.* (2020) 'CD56 regulates human NK cell cytotoxicity through Pyk2', *eLife*, 9, p. e57346. Available at: https://doi.org/10.7554/eLife.57346.

Hagen, S.J. *et al.* (2018) 'Loss of Tight Junction Protein Claudin 18 Promotes Progressive Neoplasia Development in Mouse Stomach', *Gastroenterology*, 155(6), pp. 1852–1867. Available at: https://doi.org/10.1053/j.gastro.2018.08.041.

Li, Y. *et al.* (2020) 'The α-tubulin of Laodelphax striatellus mediates the passage of rice stripe virus (RSV) and enhances horizontal transmission', *PLoS pathogens*, 16(8), p. e1008710. Available at: https://doi.org/10.1371/journal.ppat.1008710.

Tangeda, V. *et al.* (2022) 'Lon upregulation contributes to cisplatin resistance by triggering NCLX-mediated mitochondrial Ca2+ release in cancer cells', *Cell Death & Disease*, 13(3), p. 241. Available at: https://doi.org/10.1038/s41419-022-04668-1.

Wang, G. *et al.* (2020) 'NMMHC IIA triggers neuronal autophagic cell death by promoting F-actin-dependent ATG9A trafficking in cerebral ischemia/reperfusion', *Cell Death & Disease*, 11(6), p. 428. Available at: https://doi.org/10.1038/s41419-020-2639-1.